# Constraining the presence of amphibole and mica in metasomatized mantle sources through halogen partitioning experiments

Flemetakis S, Klemme S, Stracke A, Genske F, Berndt J, Rohrbach A

Corresponding author: Stamatis Flemetakis, Corrensstr. 24, 48149, Münster, Germany, Tel. +49 251 83-38397, Fax +49 251 83-33458

Email: stam.flemetakis@uni-muenster.de

Institut für Mineralogie, Westfälische-Wilhelms-Universität Münster, Corrensstrasse 24, 48149 Münster, Germany

## Abstract

We present experimentally determined partition coefficients ($D^{min/melt}$) for F and Cl between pargasite (amphibole), phlogopite (mica), clinopyroxene and basanitic melts. All experiments were performed at 1.4 GPa and temperatures between 1015°C and 1250°C to simulate fractionation of halogens during melting of metasomatized mantle. The water content of all starting materials was 16 wt.% to promote crystallization of amphibole and mica. The halogen content of all starting mixtures was 0.45 wt.% for F and 0.61 wt.% for Cl. Our data show that F is compatible ($D > 1$) in pargasite and phlogopite, while Cl is strongly incompatible ($D < 0.1$) in both phases.

The experimentally derived partition coefficients allow to quantitatively constrain the amounts of mica- and amphibole in metasomatized spinel-lherzolite sources from the observed halogen and rare earth element contents in derivative melts. Calculated F/Cl and F/Nd values of melts from different mantle sources, ranging from depleted to

fertile and metasomatized mantle, are compared to those of melt inclusions from basalts from mid ocean ridges, ocean islands, and arc and intra-plate continental settings. Our results suggest that, depending on the tectonic setting, F/Cl and F/Nd of melt inclusions can be used to determine the presence and the amount of amphibole and mica in different mantle sources, and thus allow distinguishing between melting of nominally anhydrous and volatile-rich mantle sources.

## 1. Introduction

The presence of volatile elements in the Earth's mantle significantly influences the geodynamic and geochemical evolution of our planet. Volatiles such as $H_2O$, $CO_2$, $CH_4$, or the halogens affect the mantle's solidus temperature and rheological properties, and thus are important for understanding mantle melting and dynamics (e.g., Green, 2015). Significant concentrations of volatiles, including the halogens, can be stored in mantle minerals and transported to the surface in volatile and halogen-bearing mantle-derived melts and fluids, which are typically found at convergent plate boundaries and rift settings. Hence, the flux of halogens from the mantle is important for constraining part of the Earth's volatile element cycle.

Earth's mantle has a high storage potential for halogens. Nominally anhydrous and halogen-free minerals such as olivine can store up to 0.45 wt.% F (Mosenfelder and Rossman, 2013a, 2013b; Grützner et al., 2018). The partitioning of halogens between minerals, melts and fluids shows that F and Cl are incompatible in olivine and pyroxenes with $D_F > D_{Cl}$ in all phases for both melts and fluids (Edgar and Pizzolato, 1995; Hauri et al., 2006; Beyer et al., 2012, 2016; Bernini et al., 2012; Fabbrizio et al., 2013; Dalou et al., 2012, 2014; Joachim et al., 2015, 2017). On the other hand, F-rich mantle minerals such as pargasitic amphibole and phlogopite are stable at pressures

between 0.5 to 8 GPa and temperatures between ~ 900°C to 1150°C (Green, 1973; Millhollen et al., 1974; Mysen and Boettcher, 1975a, 1975b; Mengel and Green, 1989; Wallace and Green, 1991; Niida and Green, 1999; Conceição and Green, 2004; Harlow and Davies, 2004; Adam et al., 2016), thus stable phases in the subcontinental lithosphere and the sub-arc mantle wedge. Moreover, Foley (1991) showed that the F-rich endmember of pargasite can be stable up to temperatures of ca. 1300°C. Hence, halogen-rich amphiboles and phlogopite may be residual phases during mantle melting at island-arcs and continental rifts.

Indeed, pargasitic amphiboles have been observed in spinel-, and garnet-lherzolite xenoliths (e.g. Varne, 1970; Francis, 1976; Takahashi, 1980; Dawson and Smith, 1982; Griffin et al., 1984; Nickel and Green, 1984) and in orogenic peridotites (e.g. Cawthorn, 1975; Ernst, 1978; Medaris, 1980; Obata and Morten, 1987; Seyler and Mattson, 1989), confirming that amphibole is a common accessory volatile-bearing mineral in the upper mantle (Green et al., 2010; 2014), which crystallizes during metasomatic refertilization of peridotites (Wallace and Green, 1991; Niida and Green, 1999). Phlogopite is another common accessory mantle phase, particularly in the subcontinental lithosphere (Kushiro et al., 1967). Mantle xenoliths from kimberlites (e.g. Aoki, 1975; Erlank et al., 1987) and alkali basalts (e.g. Witt-Eickschen and Kramm, 1998) often contain F-rich phlogopite (Edgar et al., 1994) with up to 8 wt.% F (Liu et al., 2011). Experimental studies showed that phlogopite is one of the most stable volatile-bearing minerals in the upper mantle (Wyllie and Sekine, 1982; Conceição and Green, 2004; Fumagalli and Klemme, 2015).

Consequently, partial melting of metasomatized amphibole and phlogopite-bearing mantle peridotite may explain the high halogen concentrations in subduction-related and intraplate alkaline lavas, e.g., ultrapotassic magmas such as lamproites and

kimberlites (Kjarsgaard et al., 2009; Abersteiner et al., 2018; Hanley and Koga, 2018; and references therein). The relative abundance of the halogens, especially F and Cl will be controlled by the abundance, melting behavior, and halogen content of amphibole and phlogopite in their mantle source. Identifying and quantifying these effects, using observed halogen concentrations and suitable mineral-melt partitioning data in mantle-derived melts, can therefore constrain the mineralogy and chemistry of their mantle sources.

We therefore investigated the behavior of halogens during partial melting of the upper mantle by experimentally determining the partitioning of halogens between pargasitic amphibole, phlogopite, and silicate melts. The resulting partition coefficients were used to examine the effects of amphibole and phlogopite on the halogen content of partial melts from metasomatized mantle sources. Our modeling results show that residual amphibole and phlogopite can generate distinct F/Cl and F/Nd values in partial melts. Comparing our modeled values with those from natural samples allows constraining the presence and amount of these phases in their mantle sources, showing that halogen concentrations (i.e., elemental ratios) in mantle melts can be used to identify the mineralogy of metasomatized mantle sources.

## 2. Experiments

### 2.1. Experimental Strategy

Experiments were performed in a basanitic system NCKFMAS + Ti ($Na_2O$ - CaO - $K_2O$ - FeO - MgO - $Al_2O_3$ - $SiO_2$). Halogens (F, Cl, Br, I) were added to all starting materials (see below). Four different basanitic starting compositions were prepared in order to investigate potential compositional effects on halogens partitioning.

Experiments were run at pressures of 1.4 GPa and temperatures between 1015 °C and 1250 °C. Halogen partition coefficients ($D^{min/melt}$) were derived from the experimental results for olivine, pyroxenes, amphibole and phlogopite.

## 2.2. Starting Materials

The four basanitic starting compositions used (Table 1), are similar to those investigated by Tiepolo et al. (2000). All the starting mixtures were prepared from analytical grade oxides ($SiO_2$, $Al_2O_3$, MgO, and $TiO_2$) and carbonates $CaCO_3$, $K_2CO_3$, $Na_2CO_3$. MgO was fired at 1000°C for 2 h and kept in a drying oven at 110°C for 24h. All starting materials were ground and mixed in an agate mortar under acetone to obtain homogeneous mixtures. The mixtures were vitrified in a Pt crucible at 1550°C for 4 hours to release $CO_2$ and absorbed water. The resulting glasses were ground and mixed again in an agate mortar, and then Fe was added as fayalite ($Fe_2SiO_4$), water as $Al(OH)_3$, and $Mg(OH)_2$ and halogens as salts (NaF, NaCl, KBr, and KI). The starting material mixtures were stored inside a desiccator at all times. Moreover, before each experiment the starting materials were dried again in a drying box (110 °C) for about 20 min.

Table 1. Starting material compositions

| | SFM1-BSN1 | SFM2-BSN1 | SFM1-BSN2 | SFM2-BSN2 |
|---|---|---|---|---|
| $SiO_2$ | 45.4(2) | 45.4(4) | 46.5(3) | 46.5(3) |
| $TiO_2$ | 3.0(1) | 3.0(1) | 1.6(1) | 1.6(1) |
| $Al_2O_3$ | 13.7(2) | 13.7(2) | 13.7(2) | 13.7(2) |
| FeO | 13.0(2) | 13.0(3) | 13.0(2) | 13.0(2) |
| MgO | 9.7(2) | 9.7(3) | 9.7(2) | 9.7(2) |
| CaO | 9.5(2) | 9.5(2) | 9.5(1) | 9.5(2) |
| $Na_2O$ | 3.9(1) | 1.7(1) | 3.9(2) | 1.65(8) |
| $K_2O$ | 1.76(7) | 4.00(6) | 1.76(1) | 4.00(8) |
| $H_2O$ (wt.%) | 16 | 16 | 16 | 16 |
| Halogens (wt.%) | | | | |
| F | 0.45 | 0.45 | 0.45 | 0.45 |
| Cl | 0.61 | 0.61 | 0.61 | 0.61 |
| Br | 0.68 | 0.68 | 0.68 | 0.68 |
| I | 0.77 | 0.77 | 0.77 | 0.77 |

The Fe source was synthetic fayalite, water was added as $Al(OH)_3$ and $Mg(OH)_2$. Halogens were added as NaF, NaCl, KBr, and KF. To measure the major element composition (wt%) of the starting material we vitrified a small aliquot of the starting powder using an Ir-strip heater at WWU. The resulting glass has lost all water and

halogens, the composition, however, agrees very well with the nominal starting material composition as indicated by the small errors (Numbers in parentheses represent two standard deviation (2-S.D.) in terms of least units cited).

## 2.3. Experimental techniques

All the experiments were performed in an end-loaded piston cylinder apparatus (Boyd and England, 1960) at the Institut für Mineralogie of the Westfälische Wilhelms-Universität Münster (WWU), Germany. About 2 mg of the starting material was pressed into $Au_{80}$-$Pd_{20}$ capsules that were about 2.5 mm long and 2 mm in diameter. The capsules were welded shut using a commercial Lampert PUK system (Lampert GmbH, Germany). The high-pressure assembly consisted of a ½" talc-pyrex-tube, a 6 mm O.D. graphite heater (material FB 254, Schunk, GmbH, Germany), two inner crushable alumina inserts (Haldenwanger GmbH, Germany) placed at the top and the bottom of the assembly (each with 6mm O.D.). The noble metal capsules were placed inside a boron nitride cylinder. Pressures were calibrated using the quartz-coesite transition (Bose and Ganguly, 1995) and the $MgCr_2O_4 + SiO_2 = MgSiO_3 + Cr_2O_3$ reaction (Klemme and O'Neill, 1997) and a friction correction of -13% was applied to the nominal pressure. Based on the aforementioned calibrations, pressures are accurate to 0.1 GPa. Experiments were run at 1.4 GPa and between 1015 °C and 1250 °C. All experiments were heated up to the initial temperature ($T_{in}$, Table 2) while increasing the pressure with a rate of 0.12 GPa /100°C and then cooled with different rates (cooling rate, Table 2) until they reached the final run temperature ($T_f$, Table 2). Temperatures were monitored with a $W_{97}Re_3$–$W_{75}Re_{25}$ thermocouple and controlled by a Eurotherm (Schneider Electric) controller. The temperatures were accurate to 10 °C. All the experimental details and run products are given in Table 2. Run durations varied

between 24 and 48 hours. The experiments were rapidly quenched and noble metal capsules were mounted into epoxy or acrylic and polished for microprobe analyses.

The experiments were unbuffered with respect to $fO_2$, and measured $FeO_t$ values reported represent $Fe^{2+}$. To support this assumption, charge balance calculations of the amphiboles (Leake et al., 1997) showed that no significant $Fe^{3+}$ ($\leq$ 0.095 a.p.f.u.) is present. The use of Au-Pd capsules prevented significant Fe-loss to the capsule (Kawamoto and Hirose, 1994; Hirose and Kawamoto, 1995). Finally, weighing the capsules before and the after the experiments indicated that there was no significant water-loss from our experiments.

Table 2. Experimental conditions and results

| Run# | Starting Material | P (GPa) | $T_{in}$ (°C) | Cooling rate (°C/min) | $T_f$ (°C) | t | phases present |
|---|---|---|---|---|---|---|---|
| SFE1-BSN1 | SFM1-BSN1 | 1.4 | 1250 | 0.1 | 1015 | 47:08 | ol, amph, gl |
| SFE2-BSN1 | SFM1-BSN1 | 1.4 | 1250 | 1 | 1015 | 21:30 | ol, cpx, amph, gl |
| SFE3-BSN1 | SFM2-BSN1 | 1.4 | 1250 | 0.1 | 1015 | 48:07 | ol, cpx, amph, opx, phl, gl |
| SFE1-BSN2 | SFM1-BSN2 | 1.4 | 1250 | 0.1 | 1015 | 47:08 | ol, cpx, amph, opx, gl |
| SFE2-BSN2 | SFM1-BSN2 | 1.4 | 1250 | 1 | 1015 | 21:30 | ol, cpx, amph, opx, phl, gl |
| SFE3-BSN2 | SFM2-BSN2 | 1.4 | 1250 | 0.1 | 1015 | 48:07 | ol, cpx, amph, phl, gl |

Abbreviations: ol = olivine, cpx= clinopyroxene, amph= amphibole, opx= orthopyroxene, phl= phlogopite and gl= glass. P = pressure (GPa), Tin = Initial run temperature, Cooling rate (C°/min), Tf= final run temperature, t = run duration (hh:min), T in °C.

## 2.4. Analytical Methods

The carbon-coated experimental run products were examined with a JEOL6610LV scanning electron microscope with EDX system and the major element concentrations of all phases were determined with a 5-spectrometer JEOL JXA 8530F electron microprobe analyzer (EMPA) at the Institute für Mineralogie at the Westfälische Wilhelms-Universität Münster (WWU). The F concentrations of minerals and glasses were determined using an analytical protocol similar to Zhang et al. (2016), and Flemetakis et al. (2020). A detailed description of the reference materials can be found in the supplementary material (Supp. 1, "EPMA reference material") This approach allowed determining the F and Cl concentrations in minerals and glasses with new calibration curves that are needed to correct for the interfering Fe on the F peak. Typical detection limits (3-S.D.) of a F analysis were ~ 48 - 65 µg/g for minerals and ~ 100 µg/g for glasses. For Cl detection limits were ~ 15 µg/g for minerals and ~ 10 µg/g for glasses.

For the halogen analysis of the minerals, the acceleration voltage was adjusted to 15kV and the beam current was 180 nA with 5 µm sized beam. The halogen content in the quenched melts was measured with a beam current of 60 nA and 10 µm sized beam. Counting times were 120 s on peak and 60 s on the background for both phases. Sanidine (Na), disthene (Al), diopside (Ca), San Carlos olivine (Mg), hypersthene (Si), rutile (Ti), and fayalite (Fe) were used as reference materials for the major element concentrations. Astimex Tugtupite, fluorite, and topaz were used as reference materials for F and Cl analyses. USNM Kakanui, and Arenal amphiboles, and USNM Scapolite and Sodalite, were used as unknows to check for F and Cl precision and accuracy, respectively, of our mineral analyses. Precision and accuracy of the glasses analyses,

for both F and Cl, was verified using VG-2, VG-A99, VG-568, BCR-2G, AC-E, GS-N, DR-N, 47963 (Kendrick et al., 2012), BIR-1G, NIST 610, NIST 612, Astimex Obsidian, GSE-1G and BHVO2-G. All standard analyses can be found in the Supplementary material. A detailed description of the analytical method for the analysis of the silicate glasses can be found in Flemetakis et al. (2020).

## 3. Results

### 3.1. Attainment of equilibrium

Several lines of evidence indicate that equilibrium between the silicate melts and mineral phases in our experiments has been attained. First, minerals and melts in our run products were homogeneous in terms of major elements and halogens (Supp. 1, Table 1). This is confirmed by the precision of EPM analyses of both silicate glasses and minerals. Note that minerals and glasses were measured in various areas of the experimental charges. Furthermore, we conducted a few detailed EPMA profile measurements across minerals and glasses, which also indicate unzoned minerals in our runs (Supp. 2, “Profiles”, Fig. 1-6). Furthermore, mass balance calculations show good agreement between starting material and experimental run products (Supp. 1, Table 3, mass balance).

We additionally used the Brey and Köhler (1990) and Putirka (2008) pyroxene thermometers to further examine the attainment of equilibrium in runs that contained both cpx and opx (Supp. 1, Tables). These thermometers yielded temperatures of 1050 ± 88 °C, and 1040 ± 50 °which are, within error, close to the final run T of 1015°C (Supp. 1, Tables). Overall, the aforementioned observations suggest that chemical equilibrium was attained in our experiments.

### 3.2. Mineral and glass halogen compositions

All experimental run products contain minerals and quenched melts (Table 2). Most minerals are euhedral to subhedral, free of inclusions, and all minerals are chemically homogeneous within analytical uncertainty. The majority of the quenched melts are glasses with homogeneous major and minor element compositions, and most glasses show no evidence for quench crystallization. Runs SFE1-BSN-1, -2, and SFE3-BSN-1, -2 contain glasses with small voids that were probably formed during the quench. Back-scattered electron images of typical run products are shown in Fig 1.

Halogen analyses of all phases of the experimental run products (phlogopite, amphibole, clinopyroxene, orthopyroxene, olivine and glasses) are given in Table 1 of the Supplementary material 1. Most of the runs contain olivine, amphibole, clinopyroxene and some contain orthopyroxene and/or phlogopite (Table 2). As expected, F concentrations in phlogopite and amphibole are high (~0.4 -1 wt.%), but orthopyroxene and olivine contain only small concentrations of F (< 42 ppm). Chlorine is incompatible in all mineral phases, but our data shows that phlogopite contains more Cl than coexisting amphibole ($Cl_{phl}$ = 450 ppm versus $Cl_{amph}$ = 330 ppm). For experiments where the melt phase did not quench to a glass (e.g., SFE1-BSN1), we assumed that the $H_2O$ abundance of the melt phase (12–25 wt.%) is similar to the electron probe deficit determined immediately after the experiment.

< ***Figure 1***>

Olivine and Orthopyroxene

Forsteritic olivine (Mg# = 96.1-99) is present in all runs, its size varies between 40 and 250 μm. Chlorine, Br and I could not be detected in any of the experimental

olivine grains. Fluorine was not detected in olivine. Orthopyroxene (opx) crystals are present in three runs (Supp. 1, Tables), with grain sizes from 20 to 80 μm. We could not detect any halogens in opx.

Amphibole

Amphiboles are pargasites and Ti-rich pargasites based on the classification of Locock (2014) (Supp. 1, Tables). Their grain sizes vary from 50 μm to 0.4 mm. Fluorine in amphibole varies between 0.38 and 1.04 wt.%. Chlorine contents range from 121 to 778 ppm and averages at 351 ± 96 ppm. Our experimental amphiboles also contain minor concentrations of I (32 to 205 ppm). Bromine was below detection limit.

Phlogopite

The experiments contain phlogopite (phl), with sizes ranging from 30 to 300 μm. The F content ranges from 0.6 to 1.2 wt.%. Chlorine contents from 292 to 990 ppm, with an average of 495 ± 244 ppm. Bromine and I concentrations were below detection limit in all the experimental samples.

Clinopyroxene

Clinopyroxene (cpx) is found in all the experimental run products. Their size ranges from 15 to 150 μm, and their composition is mainly diopside with an $X_{Di}$ varying from 0.86 to 0.93, and $X_{En}$ from 0.07 to 0.14. The F content of cpx ranges from 100 to 400 ppm (Supp. 1, Tables). Other halogens could not be detected.

Glasses

The glasses are homogeneous in terms of major element composition and F, Cl and Br contents (Supp. 1, Tables). Experiments SFE1-BSN-1, -2, and SFE3-BSN-1, -2 contained vesicles, probably due to the high amounts of water of the starting materials. As a result, the water content of the quenched melts varies from 13 to 24 wt.% depending on the mineral phases present. The silicate melt composition is basanitic (Le Maitre et al., 2005). The halogen content of the glasses varies depending on modal composition and mineral phases present, i.e., F concentrations range from ~ 0.3 to 0.9 wt.%, Cl from ~ 0.2 to 0.75 wt.%, Br from 500 to 5500 ppm and I from 1900 to 4900 ppm.

The major element and halogen compositions of all phases present in the experimental charges can be found in the Supplementary material 1.

### 3.4. Partition coefficients

We calculated F partition coefficients ($D^{min/melt}$) between amphibole, phlogopite, clinopyroxene and melts, and Cl partition coefficients between amphibole, phlogopite and melts (Table 3). The new data (Table 4) show that in all cases, mineral/melt $D_F > D_{Cl}$, and $D_F$ Phl/melt > $D_F$ Amp/melt > $D_F$ Cpx/melt, in agreement with previous experimental data (Hauri et al., 2006; O'Leary et al., 2010; Dalou et al., 2012; Dalou et al., 2014; Rosenthal et al., 2015; Van den Bleeken and Koga, 2015). Other experimental partitioning data for F between phlogopite and melt are from the pioneering study of Edgar and Pizzolato (1995), Adam and Green (2006), Adam et al. (2007; 2016), which both agree with our data. To our knowledge, no Cl partition coefficients between phlogopite and melt have been reported before. All data regarding the D values can be found in Supplementary material 1.

### 3.4.1 Fluorine

Amphibole

Our new amphibole-melt $D_F$ range from 0.61 ± 0.02 (2-S.D.) to 2.3 ± 0.16 (2-S.D.). Van den Bleeken and Koga (2015) report amphibole-melt $D_F$ of 1.18 ± 0.05 -1.85 ± 0.04 (1-S.D.) for water-rich starting compositions ($H_2O$ = 8-20 wt.%), at pressures between 1.3 and 3 GPa, and temperatures ranging from 750 to 1000°C.

In contrast, $D_F$ (amph/melt) values from Dalou et al. (2014), show that F is relatively incompatible in amphibole, as their $D_F$ range from 0.36 ± 0.066 to 0.635 ± 0.087 (1-S.D.), at 1.2 GPa pressure and between 1180 and 1200°C, for $H_2O$ contents ranging from 4.3 to 5.9 wt.%. Adam and Green (2006), and Adam et al., (2006; 2017), in a series of experiments using natural basanitic compositions determined $D_F$ (amph/melt) ranging from 1 ± 0.02 (1-S.D.) to 2, at P = 1-2 GPa and T = 1025° - 1050°C, which agrees well with out results.

Finally, Hauri et al. (2006) re-analyzed the experimental products of Adam and Green (1994), in basanitic starting compositions similar to our experiments, but lower amounts of water. Their $D_F$ amph/melt are 0.85 ± 0.04 (2-S.D.) and 1.19 ± 0.028 (2-S.D.) at P = 0.5-1.5 GPa and T = 1000° - 1050°C.

Phlogopite

Our new $D_F$ phl/melt partition coefficients range from 0.93 ± 0.08 (2-S.D.) to 2.56 ± 0.15 (2-S.D.). There are few experimental studies that contain F-bearing mica from which $D_F$ phl/melt could be calculated. Vukadinovic and Edgar (1993) conducted experiments in a F-rich system with amphibole-phlogopite-apatite and melt at 2 GPa and 900-1450°C. Their $D_F$ (phl/melt) varies from 1.25 to 2, depending on T and bulk composition. Edgar and Pizzolato (1995) determined $D_F$ of 0.68 ± 0.5 and 1.55 ± 0.1

(1-S.D.) between phlogopite and melts in a K-richterite-phlogopite-rich composition at 2 GPa and 900-1300°C. Hauri et al. (2006) present mica/melt partition coefficients ($D_F$ phl/melt, from the experiments of Adam and Green (1994), ranging from 1.64 ± 0.41 (2-S.D.) to 2.52 ± 0.4 (2-S.D.). Adam and Green (2006), and Adam et al., (2006; 2017) determined $D_F$ (phl/melt) in natural basanitic compositions, with D-values ranging from 1.9 ± 0.3 (1-S.D.) to 2.6 ± 0.1 (1-S.D.), for pressures between 2 and 2.5 GPa and temperatures between 1050 and 1100°C.

Clinopyroxene

Our calculated $D_F$ cpx/melt range from 0.013 ± 0.005 (2-S.D.) to 0.083 ± 0.036 (2-S.D.). There are numerous recent studies that reported cpx/melt partition coefficients for F ($D_F$ cpx/melt) at upper mantle conditions. Dalou et al. (2012) reported $D_F$ cpx/melt in the range of 0.0428 ± 0.0016 (1-S.D.) to 0.153 ± 0.004 (1-S.D.). Their anhydrous experiments were run at pressures between 0.8 and 2.5 GPa and at temperatures from 1265 to 1430°C. Dalou et al. (2014) reported $D_F$ (cpx/melt) from 0.114 ± 0.002 (1-S.D., 2.6 wt.% $H_2O$) to 0.083 ± 0.004 (1-S.D., 5.9 wt.% $H_2O$). Van den Bleeken and Koga (2015), calculated $D_F$ values that vary significantly between 0.059 ± 0.004 (1-S.D., minimum value) and 0.51 ± 0.05 (1-S.D., maximum value) for a pressure range of 1.6 - 3 GPa and temperatures between 750 and 1000°C. Hauri et al. (2006) reported $D_F$ cpx/melt of 0.014 ± 0.004 (2-S.D.) to 0.067 ± 0.012 (2-S.D.), and Rosenthal et al. (2015) reported $D_F$ cpx/melt of 0.029 ± 0.007 (2-S.D.) to 0.052 ± 0.005 (2-S.D.) at 1.2-3 GPa and temperature from 1300-1500°C. O'Leary et al. (2010) calculated $D_F$ of 0.005 ± 0.01 (1-S.D.) to 0.087 ± 0.004 (1-S.D.) in a high-alumina basalt. Their experiments were all conducted at 1.5 GPa and 1275°C and the $H_2O$ content varied from 2 - 4.9 wt.%, while the maximum $D_F$ comes from an almost anhydrous experiment (0.2 wt.%

$H_2O$). Finally, Beyer et al. (2016) reported cpx/melt $D_F$ values of 0.056 ± 0.005 (1-S.D.) and 0.074 ± 0.001 (1-S.D.) with an average of 0.066 ± 0.005. The pressure of their experimental runs ranged from 4 to 6 GPa and runs temperatures ranged from 1460 to 1550°C.

### 3.4.2. Chlorine

Amphibole

Our new $D_{Cl}$ values for amphibole span from 0.027 ± 0.001 (2-S.D.) to 0.22 ± 0.16 (2-S.D.) with an average of 0.075 ± 0.028 (2-S.D.). Hauri et al. (2006) reported values of $D_{Cl}$ for amphibole based on SIMS analyses of the experiments run by Adam and Green (1994), which were run between 1.3 - 3 GPa and 750-900°C. They give a range of values from 0.038 ± 0.3 (2-S.D.) to 0.046 ± 0.04. Van den Bleeken and Koga (2015) measured $D_{Cl}$ (amph/melt) at pressures of 1.3 - 3 GPa and at temperatures of 750-900°C. Their experiments yielded $D_{Cl}$ from 0.079 ± 0.004 (1-S.D.) to 1.87 ± 0.063 (1-S.D.). Dalou et al. (2014) also determined $D_{Cl}$ between amphibole and melts, at experimental conditions almost identical to ours, i.e., 1.2 GPa and 1210°C. Their experimentally derived Ds range from 0.12 ± 0.04 (1-S.D.) to 0.038 ± 0.08(1-S.D.). Adam and Green (2006), and Adam et al., (2006; 2017), calculated $D_{Cl}$ (amph/melt) ranging from 0.06 to 0.2 ± 0.02 (1-S.D.), at P from 1 to 2 GPa and T from 1025 to 1050°C.

Phlogopite

Our calculated $D_{Cl}$ values for phlogopites are between 0.074 ± 0.04 (2-S.D.) to 0.11 ± 0.04 (2-S.D.) with an average of 0.089 ± 0.059. Adam and Green (2006), and

Adam et al., (2006; 2017), determined $D_{Cl}$ (mica/melt) ranging from 0.29 ± 0.03 (1-S.D.) to 0.5 ± 0.1 (1-S.D.), at P from 2 to 2.5 GPa and T from 1050 to 1100°C.

Clinopyroxene

We could not determine $D_{Cl}$ for clinopyroxene, as Cl was always below the detection limit. Dalou et al. (2012) report values of 0.012 ± 0.001 (1 S.D.) to 0.021 ± 0.004 (1-S.D.), and Van den Bleeken and Koga (2015) report values of 0.06 ± 0.0004 (1-S.D.) to 0.505 ± 0.005 (1 S.D.).

Table 3. Our new Mineral/Melt partition coefficients of F and Cl

| Experiment | n analyses | Phase | $D_F$ | Error | $D_{Cl}$ | Error |
|---|---|---|---|---|---|---|
| SFE1-BSN1 | 27 | amph | 0.78 | 0.01 | 0.03 | 0.00 |
| SFE2-BSN1 | 45 | amph | 0.98 | 0.14 | 0.05 | 0.02 |
| SFE3-BSN1 | 15 | amph | 1.12 | 0.16 | 0.09 | 0.01 |
| SFE1-BSN2 | 4 | amph | 2.30 | 0.16 | 0.22 | 0.16 |
| SFE2-BSN2 | 7 | amph | 1.53 | 0.13 | 0.06 | 0.02 |
| SFE3-BSN2 | 21 | amph | 0.61 | 0.02 | 0.05 | 0.01 |
| SFE2-BSN1 | 19 | cpx | 0.083 | 0.036 | - | - |
| SFE3-BSN1 | 25 | cpx | 0.039 | 0.022 | - | - |
| SFE1-BSN2 | 8 | cpx | 0.048 | 0.034 | - | - |
| SFE3-BSN2 | 23 | cpx | 0.013 | 0.005 | - | - |
| SFE3-BSN1 | 32 | phl | 1.86 | 0.14 | 0.11 | 0.04 |
| SFE2-BSN2 | 3 | phl | 2.56 | 0.15 | 0.07 | 0.04 |
| SFE3-BSN2 | 33 | phl | 0.93 | 0.08 | 0.08 | 0.02 |

Errors reported are 2-S.D. propagated errors.

### 3.4.3. Variations on halogen partition coefficients

Published experimental $D_F$ (min/melt) for amphibole ($0.7 < D_F < 1.85$; (Edgar and Pizzolato, 1995; Hauri et al., 2006; Adam and Green, 2006; Adam et al., 2007; Dalou et al., 2014; Van den Bleeken and Koga, 2015; Adam et al., 2017) are in good agreement with our data, i.e., $0.61 < D_F < 2.3$. Our experimental data also show that F in amphibole can be incompatible ($D_F < 1$) and compatible ($D_F > 1$) depending on the Ti content in amphibole (Figure 2, top left). In amphibole with low Ti content of ~ 0.24 a.p.f.u. (amphibole cation distribution in Supp. 1, sheet 2), F is incompatible ($D_F = 0.61$) but with increasing concentrations of Ti in amphibole F becomes compatible. Only amphiboles in sample SFE2-BSN2 (Leake et al., 1997) showed indications for small concentrations of $Fe^{3+}$ ($0.062 < XFe^{3+} < 0.2$ a.p.f.u., Supp. 1, sheet 2, "Amph_$Fe^{3+}$"). Fluorine partition coefficients between phlogopite and melts in our runs vary between $0.93 < D_F < 2.56$ (Figures 2 bottom left and 2 bottom right). Our new experimental data shows that there is a positive correlation ($R^2 = 0.9535$) between the amount of Na in the interlayer site of the phlogopite structure with $D_F$ and, consequently, a negative correlation ($R^2 = 0.8861$) between K and $D_F$ (phlogopite cation distribution in Supp. 1, Tables).

Additionally, $D_F$ of amphibole and mica in the experiments where both phases are present, show a linear positive correlation ($R^2 = 0.99$), indicating that their $D_F$ behave in a similar way (Figure 2, top right).

***< Figure 2>***

Invariably, F in clinopyroxene is incompatible based on our experimental results, with $0.013 < D_F < 0.083$, which agrees well within published experimental values that range from 0.005 to 0.5 (Hauri et al., 2006; O'Leary et al., 2010; Dalou et al., 2012; Dalou et al., 2014; Rosenthal et al., 2015; den Bleeken and Koga, 2015; Beyer et al., 2016). Our experimental data indicate that $D_F$ depends on the composition of clinopyroxene (Figure 3a and 3b), as $D_F$ increases from 0.013 ± 0.002 (2-S.D.) to 0.083 ± 0.003 (2-S.D.) with increasing amount of $^{IV}Al^{3+}$ (0.052 - 0.33 a.p.f.u.) and $^{VIII}Ti^{4+}$ (0.02 - 0.105 a.p.f.u.) in clinopyroxene (clinopyroxene cation distribution in Supp. 1, Tables). These correlations indicate the control that properties, like the ionic radius of trivalent and tetravalent cations, exert on the structural sites of clinopyroxene and subsequently on the partition coefficient (for a discussion see Adam and Green, 2006; Adam et al., 2007), in this case of F.

< ***Figure 3***>

No systematic trends were observed for $D_{Cl}$ mineral-melt partition coefficients with major element compositions or any other parameters for amphibole, mica and clinopyroxene.

## 4. Discussion

### 4.1. Partial melting of amphibole or mica-bearing mantle

Amphibole and phlogopite are common accessory phases in metasomatized mantle peridotite (e.g., Harte, 1983), and are stable over a wide range of pressures and temperature in the mantle (Wallace and Green, 1991; Sato et al., 1997; Niida and Green, 1999; Conceição and Green, 2004; Condamine and Médard, 2014; Condamine et al.,

2016). As mantle amphibole and mica can contain high concentrations of halogens (Liu et al., 2011; Hanley and Koga, 2018; Frezzoti and Ferrando, 2018; Piper et al., 2019, and references therein), we will investigate whether amphibole and phlogopite control the halogen content in partial melts from metasomatized amphibole and phlogopite-bearing mantle sources. Note that apatite can also be stable in metasomatized mantle rocks and partial melting of apatite-bearing mantle rocks may also contribute to the F and Cl budget of melts derived from metasomatized peridotite. To our knowledge though, appropriate melting reactions for the presence of apatite in such systems, are not available in the literature, and therefore, we could not address the effect of apatite in our models.

Fluorine, for example, is incompatible in olivine, pyroxenes and spinel but compatible in amphibole and phlogopite. Chlorine is incompatible in all these phases. A depleted mantle (DM) source (amphibole and mica-free), with a F content of 12 ppm and a Cl content of 0.5 ppm (Salters and Stracke, 2004) will have a F/Cl = 24 ± 4.5 (1-S.D.). On the other hand, metasomatic influx of volatiles, will lead to increasing F and Cl concentrations, and F and Cl may be stored in mantle amphibole and phlogopite. Fluorine and Cl concentrations in such an amphibole-, phlogopite-bearing source are expected to increase with the modal amounts of amphibole and phlogopite. On the other hand, melts derived from an amphibole- and/or phlogopite bearing mantle source, will show lower F/Cl values of the mantle. Therefore, such variations of the F/Cl values of the partial melts can be indicative of the presence of amphibole and mica in a mantle source. The same principle can be applied to the F/Nd values of partial melts. Workman et al. (2006) proposed that F is similarly incompatible to Nd during anhydrous mantle melting (i.e., without amphibole or mica in the source), on the basis of constant F/Nd of ocean island basalts and MORB (F/Nd = 21.7 ± 2.6 (2-S.D.). During partial melting

of amphibole or mica-bearing mantle sources, $D_F > 1$, but $D_{Nd} << 1$, resulting in $D_F/D_{Nd} > 1$. Consequently, deviations of the relatively invariable F/Nd in basalts are thus expected for partial melting of amphibole or mica-bearing mantle sources. These deviations can therefore be used identify melting of amphibole-, and mica-bearing mantle sources.

Furthermore, as amphibole and mica are probably of metasomatic origin, the halogen signature of partial melts may be used in order to decipher the nature and mineralogy of the metasomatized mantle sources.

**4.2. Modelling partial melting of variably metasomatized mantle sources**

Partial mantle melting is modeled by incremental non-modal melting with small melt increments (0.0001%, cf. Stracke et al., 2003).

For melting of anhydrous, that is, amphibole- and phlogopite-free spinel lherzolite, we use a DM mantle composition with initial F, Cl, and Nd contents of 12 ppm, 0.5 ppm and 0.713 ppm (Salters and Stracke, 2004) and a more enriched mantle source (EM) with 31 ppm of F, 22 ppm of Cl and 1.25 ppm of Nd after Shimizu et al. (2016 (Table, 4). The melting reactions and initial mineral abundances were taken from Brown and Lesher (2016, Table 6).

To model melting of metasomatized mantle sources, we used different amphibole and/or phlogopite mineral modal abundances from 2% to up to 13% (Table 4) and F-Cl contents for these phases in the source, from 60 ppm to 1wt.%. Details of the halogen contents and modal abundance of each individual phase, and in each distinct model can be found in Table 4. Melting reactions for metasomatized mantle are taken from Holloway and Burnham (1972) for amphibole-bearing sources, and Condamine and Médard (2014) for amphibole and phlogopite-bearing sources.

The F and Cl content of amphibole for each modeled metasomatized mantle source has been determined by mass balance, using an average F content of 0.64 wt.% and 0.037 wt.% for Cl. Note that these values agree well with natural mantle amphibole compositions (GEOROC database, Amphibole spreadsheet; Frezzoti and Ferrando, 2018). The F and Cl content of phlogopite for each modeled metasomatized mantle source has been determined by mass balance, using an average content of 0.97 wt.% for F and 0.047 wt.% for Cl, also in good agreement with natural concentrations of these elements in phlogopite (GEOROC database, Mica spreadsheet; Frezzoti and Ferrando, 2018).

We also assume that the entire halogen content of the source is contained in amphibole and phlogopite, a valid assumption as nominally F-free minerals such as olivine and the pyroxenes contain only a few ppm F and only about 1 ppm Cl (Beyer et al., 2012; Grützner et al., 2017), which is negligible compared to the high halogen contents of amphibole and phlogopite.

Furthermore, the Nd content of the source is assumed to be contained in amphibole, phlogopite and clinopyroxene. We use the concentrations of amphiboles (13.7 ppm), phlogopites (0.29 ppm) and clinopyroxenes (12.3 ppm) in metasomatized spinel lherzolites reported by Ionov and Hofmann (1995). The former assumption is valid as natural olivines (~173k out of the total ~174k analyses of olivines in GEOROC database, contain no Nd) and orthopyroxenes (~35k out of the total ~41k analyses of orthopyroxenes in GEOROC database contain no Nd contents) do not contain significant concentrations of Nd.

Mica and amphibole-bearing mantle rocks are the source of many ultra-potassic magmas (Edgar et al., 1976; Edgar et al., 1980; Arima and Edgar, 1983a, b; Waters, 1987), and thus we also modeled partial melting of F-rich phlogopite (and amphibole)

-bearing lherzolite source. In these models, our lherzolite source contains 4% modal phlogopite and 1% amphibole. Phlogopite is more abundant than amphibole in this case, as it is the most probable candidate to deliver the high-K contents of these magmas (Foley and Peccerillo, 1992; and references therein).

For examining the source of ultra-potassic magmas, we modeled three distinct sources. The modelled sources have the same F (830 ppm), and Nd (4.9 ppm) contents but different Cl contents, i.e., 83 ppm for source (a), 124.5 ppm for source (b), and 166 ppm for source (c), (c.f., Table 4). These contents are similar to those of South African MARID xenoliths, (Dawson and Smith, 1977; Waters, 1987; Fitzpayne et al., 2019). Note that Cl shows a relatively narrow range in natural MARID samples i.e., 0.006 to 0.03 wt.% in amphiboles (Giuliani et al., 2013; Banerjee et al., 2018; Fitzpayne et al., 2018) and 0.01 to 0.03 wt.% in mica (phlogopite) (Wagner et al., 1996; Banerjee et al., 2018; Fitzpayne et al., 2018) compared to F (0.1 – 1.7 wt.% in amphibole after Giulani et al., 2013; Banerjee et al., 2018; Fitzpayne et al., 2018, and 0.01 to 1.1 wt.% in mica after Wagner et al., 1996; Banerjee et al., 2018; Fitzpayne et al., 2018).

Table 4. Modal amounts and halogen contents (ppm) of minerals of the modeled sources

| Sources | Mineral modal amounts | F | Cl | Nd |
|---|---|---|---|---|
| **Depleted Mantle source (DM)** | | | | |
| Ol | 57 | 0 | 0 | 0 |
| Opx | 25.5 | 0 | 0 | 0 |
| Cpx | 15 | 0 | 0 | 0 |
| Sp | 2.5 | 0 | 0 | 0 |

| | | | | |
|---|---|---|---|---|
| Total (source) | 100 | 12 | 0.5 | 0.71 |
| **Enriched Mantle source (EM)** | | | | |
| Ol | 57 | 0 | 0 | 0 |
| Opx | 25.5 | 0 | 0 | 0 |
| Cpx | 15 | 0 | 0 | 0 |
| Sp | 2.5 | 0 | 0 | 0 |
| Total (source) | 100 | 31 | 22 | 1.25 |
| **1 amph - 1 mica - Metasomatized Mantle source** | | | | |
| Ol | 51.37 | 0 | 0 | 0 |
| Opx | 19.26 | 0 | 0 | 0 |
| Cpx | 26.74 | 0 | 0 | 3.3 |
| Amph | 1.00 | 64 | 3.73 | 0.14 |
| Phl | 1.00 | 90.70 | 4.73 | 0.003 |
| Sp | 0.63 | 0 | 0 | 0 |
| Total (source) | 100 | 154.7 | 8.46 | 3.43 |
| **4 amph - 1 mica - Metasomatized Mantle source** | | | | |
| Ol | 49.8 | 0 | 0 | 0 |
| Opx | 18.7 | 0 | 0 | 0 |
| Cpx | 25.9 | 0 | 0 | 3.2 |

| | | | | |
|---|---|---|---|---|
| Amph | 4 | 256 | 14.9 | 0.5 |
| Phl | 1 | 90.7 | 4.7 | 0.0 |
| Sp | 0.6 | 0 | 0 | 0 |
| Total (source) | 100 | 346.7 | 19.65 | 3.74 |
| **5 amph - Metasomatized Mantle source** | | | | |
| Ol | 49.8 | 0 | 0 | 0 |
| Opx | 18.7 | 0 | 0 | 0 |
| Cpx | 25.9 | 0 | 0 | 3.2 |
| Amph | 5 | 320 | 18.7 | 0.7 |
| Phl | 0 | 0 | 0 | 0 |
| Sp | 0.6 | 0 | 0 | 0 |
| Total (source) | 100 | 320 | 18.65 | 3.87 |
| **8 amph - 2 mica - Metasomatized Mantle source** | | | | |
| Ol | 47.2 | 0 | 0 | 0 |
| Opx | 17.7 | 0 | 0 | 0 |
| Cpx | 24.6 | 0 | 0 | 3.0 |
| Amph | 8 | 512 | 29.8 | 1.1 |
| Phl | 2 | 181 | 9 | 0 |
| Sp | 0.6 | 0 | 0 | 0 |

| | | | | |
|---|---|---|---|---|
| Total (source) | 100 | 693.4 | 39.3 | 4.12 |
| **10.5 amph - 2.9 mica - Metasomatized Mantle source** | | | | |
| Ol | 45.3 | 0 | 0 | 0 |
| Opx | 17.0 | 0 | 0 | 0 |
| Cpx | 23.1 | 0 | 0 | 2.9 |
| Amph | 10.5 | 672 | 39.2 | 1.4 |
| Phl | 2.9 | 263 | 14 | 0 |
| Sp | 1.1 | 0 | 0 | 0 |
| Total (source) | 100 | 935.03 | 52.88 | 4.35 |
| **1 amph - 4 mica – F-rich source (a)** | | | | |
| Ol | 49.8 | 0 | 0 | 0 |
| Opx | 18.7 | 0 | 0 | 0 |
| Cpx | 25.9 | 0 | 0 | 27 |
| Amph | 1 | 1000 | 100 | 3.11 |
| Phl | 4 | 1000 | 100 | 0.17 |
| Sp | 0.6 | 0 | 0 | 0 |
| Total (source) | 100 | 830 | 83 | 4.9 |
| **1 amph - 4 mica – F-rich source (b)** | | | | |
| Ol | 49.8 | 0 | 0 | 0 |

| | | | | |
|---|---|---|---|---|
| Opx | 18.7 | 0 | 0 | 0 |
| Cpx | 25.9 | 0 | 0 | 27 |
| Amph | 1 | 1000 | 150 | 3.11 |
| Phl | 4 | 1000 | 150 | 0.17 |
| Sp | 0.6 | 0 | 0 | 0 |
| Total (source) | 100 | 830 | 124.5 | 4.9 |
| **1 amph - 4 mica – F-rich source (c)** | | | | |
| Ol | 49.8 | 0 | 0 | 0 |
| Opx | 18.7 | 0 | 0 | 0 |
| Cpx | 25.9 | 0 | 0 | 27 |
| Amph | 1 | 1000 | 200 | 3.11 |
| Phl | 4 | 1000 | 200 | 0.17 |
| Sp | 0.6 | 0 | 0 | 0 |
| Total (source) | 100 | 830 | 166 | 4.9 |

Modal amounts of metasomatized sources with different initial amphibole and phlogopite abundances. We maintained the same relative proportions of the other phases present (i.e. olivine, opx, cpx and spinel) after Brown and Lesher (2016). The F, Cl and Nd mineral/melt partition coefficients, used in the melting model, are given in Table 5.

Mineral/melt partition coefficients used in the melting model are listed in Table 5. We used available Nd $D_{min/melt}$ values from the literature (Kennedy et al., 1993; Salters

and Longhi, 1999; Lundstrom et al., 1998; LaTourrette et al., 1995) for all the mineral phases. As to F and Cl, we used literature $D_{min/melt}$ values for olivine and orthopyroxene (Hauri et al., 2006; Dalou et al., 2014), and $D_F$ (cpx/melt) of our experimental results. Although Al and Ti content of clinopyroxene influences $D_F$ (cpx/melt), this has only a very small effect, if any, on the calculated melt compositions, because $D_F$ (cpx/melt) << 1. We used the $D_{Cl}$ (cpx/melt) reported by Dalou et al. (2014). As we have shown in the experimental part, $D_F$ (amph/melt) ranges from incompatible ($D_F$ ~ 0.61) to highly compatible ($D_F$ ~ 2.3) and similar behavior was observed for phlogopite ($D_F$ ~ 0.93 to ~ 2.6). To address these variable $D_F$ and $D_{Cl}$, we modeled the metasomatized mantle sources (MM) using both $D_F > 1$ and $D_F < 1$ for both phases. In both cases we chose values from our experimental runs where both phases are present (i.e., SFE3-BSN1, and SFE3-BSN2). $D_{Cl}$ for amphibole and mica showed no compositional dependence on our experimental runs and as such we used the average values of our data.

Table 5. Partition coefficients used in the melting model

| Minerals | Olivine | Orthopyroxene | Clinopyroxene | Amphibole | Mica | Amphibole | Mica |
|---|---|---|---|---|---|---|---|
| $D_F$ | 0.0025 [2] | 0.027 [2] | 0.045 [1] | 1.12 [1] | 1.86 [1] | 0.61[1*] | 0.93[1*] |
| $D_{Cl}$ | 0.003 [2, 3] | 0.0042 [3] | 0.013 [3] | 0.075 [1] | 0.089 [1] | 0.075 [1] | 0.089 [1] |
| $D_{Nd}$ | 0.00042 [4] | 0.012 [5] | 0.065 [4] – 0.18 [6] | 0.25 [7] | 0.012 [7] | 0.25 [7] | 0.012 [7] |

[1] present study; [1*] present study, $D_F < 1$ for amphibole and mica; [2] Hauri et al. (2006); [3] Dalou et al. (2014); [4] Kennedy et al. (1993); [5] Salters and Longhi (1999); [6] Lundstrom et al. (1998); [7] LaTourrette et al. (1995).

### 4.3. F and Cl melting model

#### 4.3.1. Bimodal behavior of F in amphibole and mica

Our experimental data shows that F can be both compatible and incompatible in amphibole and mica. In the melting models presented next, we will first examine the partial melting of sources with amphibole and mica, with a $D_F > 1$ for both phases. Then we will compare these results with those using $D_F < 1$ for both phases.

The F contents of partial melts for metasomatized sources where F is compatible in both amphibole and mica, are plotted against their F/Cl for different degrees of partial melting (Fig. 4), and compared to those from anhydrous sources, i.e., amphibole- and mica-free depleted mantle (DM) and enriched mantle (EM). F/Cl increase in melts from DM, until all F and Cl is released into the melts when the degree of melting (*F*) > 15 % and F/Cl ~ 25. Partial melting of the EM source produces melts lower F/Cl of ~ 1.4, due to DF ≈ DCl (i.e., olivine, pyroxenes and spinel) over a greater range of F contents compared to melts from DM.

In contrast, partial melting of variably amphibole- and/or phlogopite-bearing mantle sources (Fig. 4), produces melts with a max of F/Cl ~ 17 and higher F contents compared to anhydrous melts from both DM and EM. This is because F is compatible in both amphibole and phlogopite ($D_F$ >1), while Cl is incompatible ($D_{Cl} < 0.1$).

< ***Figure 4*** >

However, F/Cl in melts from metasomatized sources differ for variable source abundances of amphibole and mica. The F content of the metasomatized source increases with increasing initial abundance these, and accordingly, the F contents of the partial melts also increase. The F/Cl depend in the relative abundance of amphibole and mica for each source and decreases with increasing amphibole/mica ratio at constant F.

The abundance of mica has a greater influence on the F-content of the derived melts than the abundance of amphibole, because $D_F$ phlogopite > $D_F$ amph. As a result, sources with more phlogopite have higher F contents, thus the melts extracted will have higher F contents as long as phlogopite remains residual (Fig. 4). After phlogopite is exhausted, the F content of the melt starts to decrease with increasing degree of partial melting. In sources that contain only amphibole (source "5-amph" in Fig. 4), the F content of the melt decreases from the onset of melting until amphibole is consumed. Afterwards, the F/Cl remains constant since both elements become similarly incompatible.

**< *Figure 5* >**

However, when we use $D_F < 1$ for both amphibole and phlogopite, melts from the different metasomatized sources evolve differently (Fig. 5). In this case, melts have higher fluorine contents for the same degree of melting compared to melts with $D_F > 1$, as $D_F/D_{Cl}$ is decreasing (Fig. 5). As a result, melts show a different evolution as higher concentrations of F and Cl are released into the melts. This is evident especially for low degrees of partial melting, i.e., up to F ~ 5%. Hence, for low degrees of partial melting, the different $D_F$ of mica and amphibole (resulting into a lower $D_F/D_{Cl}$ of the source) will generate distinct signatures for different concentrations of F in the melts.

Overall, $D_F$ of amphibole and mica exert a great influence on the $D_F/D_{Cl}$ of the source, and subsequently on the F and F/Cl values of partial melts. These differences can be identified on a F vs F/Cl plot of halogen contents of melts. When applied in natural samples, such a plot can constrain the mineralogy and halogen content of individual mantle sources. However, as experimental and natural data have shown that

F is predominantly compatible in amphibole (Edgar and Pizzolato, 1995; Hauri et al., 2006; Van den Bleeken and Koga, 2015; Bénard et al., 2017) and mica (Edgar and Pizzolato, 1995; this study), hence, models in the following sections will examine the F/Cl of melts with $D_F > 1$ for both mica and amphibole.

### 4.3.2. Fluorine-rich mantle sources

We also explored sources that may be related to the generation of ultra-potassic magmas (Table 5, "1 amph- 4 mica, F-rich sources" (a), (b), and (c)). These sources produce extremely F-rich partial melts (8500-9000 ppm), even at low degrees of partial melting ($F$ < 5%) due to the high F content of both amphibole and mica (1000 ppm F each, table 5). Since $D_F/D_{Cl} >> 1$, the F contents of the melts start to decrease when mica melts out (~5% melting), and when amphibole melts out (~8% melting), F contents decrease sharply. The sources we examined contain the same amount of F but increasing concentrations of Cl, i.e., 83 -166 ppm.

< ***Figure 6*** >

### 4.3.3. F and Nd melting model

Similar to F and Cl, F and Nd concentrations of partial melts can be used to trace volatile-bearing minerals in a mantle source. Fluorine is compatible in both amphibole and mica while Nd is incompatible. The concentrations of F and Nd in partial melts derived from different metasomatized sources are shown in Fig. 7.

< ***Figure 7*** >

Anhydrous mantle sources, both DM and EM (Fig. 7) produce melts with relatively invariable F/Nd that is relatively close to their source value, owing to $D_F/D_{Nd}$ ~ 1 (Table 6).

Melts derived from metasomatized sources generally have much higher F/Nd up to ~ 212, compared to melts from DM (F/Nd ≈ 17) or EM (F/Nd ≈ 25). The F/Nd of the partial melts increases with increasing degree of melting. This is due to amphibole and mica which are consumed quickly during melting, thus contributing high F amounts to the melts, while the Nd content is controlled by residual clinopyroxene. Moreover, mica seems to exert a more significant role on the F content and F/Nd of the partial melts than amphibole, because $D_F$ mica > $D_F$ amph. This can be observed in the melting curves of the mica-bearing sources. (Fig. 7). As long as mica remains residual, the F content of the melts increases. At the locus where mica melts out, the F content of the melts starts to decrease, and the melting curves begin to have negative slopes. $D_F/D_{Nd}$ remain greater unity, until both amphibole and mica have melted out. At the point where both phases are consumed, F/Nd becomes constant owing to $D_F \approx D_{Nd}$ in the remaining phases (olivine, pyroxenes and spinel) and the melts generated approach the F/Nd of the source.

Melts from F-rich sources (grey area in Fig. 7) behave similarly to those from metasomatized sources, though with higher F concentrations (e.g., 8500-9000 ppm for F < 5%).

**4.3.3. Melting model compared to natural melt inclusion data**

Whether volatile-rich continental rift or arc-related basalts originate from anhydrous or metasomatized mantle sources is often debated. Moreover, whether

amphibole or mica are the main hosts of the volatile content in the metasomatized source of these magmas is often ambiguous (Gazel et al., 2012).

In Figure 8 we compare our modeled F contents, F/Cl and F/Nd values, to melt inclusion data from different geotectonic settings.

< ***Figure 8*** >

F/Cl and F/Nd values of olivine-hosted melt inclusions in MORB (Shimizu et al, 2019) range from < 1 to ~25, for F/Cl, and ~10 to 50, for F/Nd, and plot inside the predicted range for a typical DM(-EM) melts (Fig. 8).

Melt inclusions from OIBs (Métrich et al., 2014; Cabral et al., 2014) with F/Cl ~ 4 and F contents of ~ 500 to 1500 ppm, plot outside the modeled range for melts from 'metasomatized mantle' sources (Fig. 8). This suggests the absence of amphibole and mica from their respective sources, which agrees with the estimated temperatures and pressure conditions of OIB sources (Green et al., 2001; Falloon et al., 2007), that typically exceed the thermal stability of amphibole and mica (Mengel and Green, 1989; Niida and Green 1999). The F/Nd values of melt inclusions from OIB (Métrich et al., 2014; Cabral et al., 2014) range from ~ 20 – 35 (Pico Island, Azores, Mangaia, Cook Islands) with almost similar F contents (900 to 1500 ppm). The relatively small variation in F/Cl (~ 2 to 4), F/Nd values (~ 20 to ~ 40), and F contents (between 900 and 1500 ppm), from these two different OIB sources suggests that their mantle reservoirs may have comparable halogen contents, and that shallow processes, e.g. diffusion, contamination, has a negligible or similar effect on the values.

Gazel et al. (2012) reported F, Cl and Nd melt inclusion data from the Big Pine Volcanic Field in the Basin and Range province in the USA (Fig. 8). The genesis of the

alkaline basalts in the area is debated (c.f., Gazel et al., 2012; Putirka and Platt, 2012), but, their halogen content has been attributed to residual mica and/or amphibole in their mantle source, based on $H_2O/K_2O$ of melt inclusions (Wallace and Anderson, 1998). The F/Cl values of these magmas show a narrow range (~ 3.5 to 7), while their F content ranges from ~ 50 to ~ 3000 ppm. Melt inclusions with the highest F content (~ 2800-3000 ppm) plot inside our modeled field for "metasomatized mantle" (Fig. 8). Additionally, the degree of melting assumed for the melts, ~3 - 10% (Gazel et al., 2012) agrees very well with our calculated melting curves, for a metasomatized source with < 5% of these minerals present. The F/Nd from the same dataset ranges from ~ 20 to 40, but, in contrast to the F/Cl, they plot outside our "metasomatized mantle" (Fig. 8). Only the melt inclusions with the highest F content (~ 2800 ppm) plot close to our modeled source containing 1% of amphibole and mica. This may indicate the presence of small amounts of amphibole and/or phlogopite in the source of these magmas. Thus, we suggest that F-Cl and/or F-Nd systematics (F/Cl, F/Nd and F content of melts) can be applied to identify metasomatized mantle sources and to place constraints on the presence and amount of amphibole and mica in the source of the magmas, as opposed to other volatile data ($H_2O/K_2O$).

Arc melt inclusion data span a wide range of F contents from 100 ppm to > 8500 ppm with F/Cl values < 3.5 and fall into two distinct groups. The first group comprises melt inclusions in basalts from Kamchatka (Portnyagin et al., 2007) and the Aeolian Islands (Rose-Koga et al., 2012). They have F/Cl between < 1 and 2.5 and F concentrations from ~ 100 ppm to around 1200 ppm, which plot far away from modeled melt compositions for metasomatized mantle sources (Fig. 8). The F/Nd values for melt inclusions from Kamchatka range between 18 to 73, for F contents between 200 to ~500

ppm (Portnyagin et al., 2007), while for the Aeolian Islands F/Nd values range from 15 to 45 and F contents from 300 to 1200 ppm (Rose-Koga et al.,2012). In both plots (F/Cl vs F, and F/Nd vs F), data cluster away from our modeled metasomatized sources, thus confirming the absence of amphibole and mica from the source of the magmas (Portnyagin et al., 2007; Rose-Koga et al., 2012).

Group two comprises melt inclusions data from ultra-potassic rocks in the Western-Transmexican Volcanic Belt. They have F/Cl from ~ 2 to 5, F/Nd from ~ 50 to 120, and F from 4000 to >8500 ppm. Melt inclusion data with F contents of ~ 4000 to 4800 ppm agree well with our modeled low degree partial melts (< 2.5 %) from metasomatized mantle containing considerable amounts (5 to 13%) of amphibole and/or mica. Melt inclusions with F contents > 5000 ppm agree very well with our modeled F-rich sources for intermediate degrees of partial melting (< 5%) and a Cl content of 166 ppm for the source (Fig. 8). Further, the $K_2O$ content and K/La in olivine-hosted melt inclusions in the lavas indicate that residual phlogopite is present in the source of the magmas during melting (Vigoroux et al., 2008). Additionally, amphibole phenocrysts have been reported in lamprophyres from the same area (Allan and Carmichael, 1984). Based on the summary of the above observations, we argue that our model predicts not only the presence but also the relative abundance of amphibole and phlogopite in the source of these high-K magmas from the Western-Transmexican Volcanic Belt.

Our models therefore suggest that amphibole- and mica-bearing lherzolites with relatively high concentrations of F and moderate Cl and Nd, and MARID-like sources with very high concentrations of F and Cl, can generate the F/Cl and F/Nd signatures found in high-K magmas as in the Transmexican Volcanic Belt (Vigoroux et al., 2008).

This is the first time that F-Cl systematics have been used to distinguish the sources of such magmas.

In summary, the above-mentioned examples of natural data from different settings demonstrate that our model can be used to constrain not only the presence of amphibole and mica in the source of the magmas but also their relative amount.

## Conclusions

We present a new set of experimentally determined F and Cl partition coefficients for amphibole, mica, clinopyroxene and basanitic melts. Fluorine is much more compatible than Cl in mica and amphibole.

The experimentally determined partition coefficients were used in a melting model to calculate F/Cl and F/Nd of partial melts for different peridotite sources, ranging from a depleted MORB mantle source to metasomatically enriched mantle compositions. We compare our modeled melt compositions with natural melt inclusion data from different geotectonic settings and we find that our model can be used to constrain not only the presence of amphibole and mica in the mantle source of the magmas but also their relative amount.

## Acknowledgements

Our thanks go M. Feldhaus, J. Kemmann, M. Trogisch, B. Schmitte, and P. Weitkamp for excellent sample preparation, and maintenance and repairs of the experimental and analytical facilities at the Institut für Mineralogie at WWU Münster. Comments by M. Willig and C. Renggli are greatly appreciated. Our thanks go to J. Adam for a constructive review which helped to substantially improve the paper. We acknowledge

funding by the Deutsche Forschungsgemeinschaft (DFG -SFB-TRR 170 publication no. 118)

## References

Adam, J., Green, T.H., 1994. The effects of pressure and temperature on the partitioning of Ti, Sr and REE between amphibole, clinopyroxene and basanitic melts. Chemical Geology 1–15.

Adam, J., Green, T.H., 2006. Trace element partitioning between mica- and amphibole-bearing garnet lherzolite and hydrous basanitic melt: 1. Experimental results and the investigation of controls on partitioning behaviour. Contributions to Mineralogy and Petrology 152, 1–17. https://doi.org/10.1007/s00410-006-0085-4

Adam, J., Oberti, R.C., Green, T.H., 2007. An electron microprobe, LAM-ICP-MS and single-crystal X-ray structure refinement study of the effects of pressure, melt-H2O concentration and fO2 on experimentally produced basaltic amphiboles. ejm 19, 641–655. https://doi.org/10.1127/0935-1221/2007/0019-1750

Adam, J., Turner, M., Hauri, E.H., Turner, S., 2016. Crystal/melt partitioning of water and other volatiles during the near-solidus melting of mantle peridotite: Comparisons with non-volatile incompatible elements and implications for the generation of intraplate magmatism. American Mineralogist 101, 876–888. https://doi.org/10.2138/am-2016-5437

Aoki, K., 1975. Origin of phlogopite and potassic richterite bearing peridotite xenoliths from South Africa. Contributions to Mineralogy and Petrology 53, 145–156.

Arima, M., & Edgar, A. D., 1983. High Pressure Experimental Studies on a Katungite and their Bearing on the Genesis of some Potassium-Rich Magmas of the West Branch of the African Rift. Journal of Petrology 24(2), 166–187.

Arima, M., & Edgar, A. D., 1983. A high-pressure experimental study on a magnesian-rich leucite-lamproite from the West Kimberley area, Australia: petrogenetic implications. Contributions to Mineralogy and Petrology 84(2), 228–234.

Banerjee, S., Kyser, T.K., Mitchell, R.H., 2018. Oxygen and hydrogen isotopic composition of phlogopites and amphiboles in diamond-bearing kimberlite hosted MARID xenoliths: Constraints on fluid-rock interaction and recycled crustal material in the deep continental lithospheric mantle. Chemical Geology 479, 272–285. https://doi.org/10.1016/j.chemgeo.2018.01.022

Bénard, A., Koga, K.T., Shimizu, N., Kendrick, M.A., Ionov, D.A., Nebel, O., Arculus, R.J., 2017. Chlorine and fluorine partition coefficients and abundances in sub-arc mantle xenoliths (Kamchatka, Russia): Implications for melt generation and volatile recycling processes in subduction zones. Geochimica et Cosmochimica Acta 199, 324–350. https://doi.org/10.1016/j.gca.2016.10.035

Bernini, D., Wiedenbeck, M., Dolejš, D., Keppler, H., 2012. Partitioning of halogens between mantle minerals and aqueous fluids: implications for the fluid flow regime in subduction zones. Contributions to Mineralogy and Petrology 165, 117–128. https://doi.org/10.1007/s00410-012-0799-4

Beyer, C., Klemme, S., Grützner, T., Ireland, T.R., Magee, C.W., Frost, D.J., 2016. Fluorine partitioning between eclogitic garnet, clinopyroxene, and melt at upper

mantle conditions. Chemical Geology 437, 88–97. https://doi.org/10.1016/j.chemgeo.2016.05.032

Beyer, C., Klemme, S., Wiedenbeck, M., Stracke, A., Vollmer, C., 2012. Fluorine in nominally fluorine-free mantle minerals Experimental partitioning of F between olivine, orthopyroxene and silicate melts with implications for magmatic processes. Earth and Planetary Science Letters 337–338, 1–9. https://doi.org/10.1016/j.epsl.2012.05.003

Bose, K., Ganguly, J., 1995. Quartz-coesite transition revisited: Reversed experimental determination at 500–1200 °C and retrieved thermochemical properties. American Mineralogist 80, 231–238.

Boyd, F.R., England, J.L., 1960. Apparatus for phase-equilibrium measurements at pressures up to 50 kilobars and temperatures up to 1750°C. Journal of Geophysical Research: Solid Earth 65, 741–748. https://doi.org/10.1029/JZ065i002p00741

Brey, G.P., Köhler, T., 1990. Geothermobarometry in Four-phase Lherzolites II. New Thermobarometers, and Practical Assessment of Existing Thermobarometers. Journal of Petrology 31, 1353–1378.

Brown, E.L., Lesher, C.E., 2016. REEBOXPRO: A forward model simulating melting of thermally and lithologically variable upwelling mantle. Geochemistry, Geophysics, Geosystems 17, 3929–3968. https://doi.org/10.1002/2016GC006579

Cawthorn, R.G., 1975. The Amphibole Peridotite-Metagabbro Complex, Finero, Northern Italy. The Journal of Geology 83, 437–454. https://doi.org/10.1086/628121

Conceição, R.V., Green, D.H., 2004. Derivation of potassic (shoshonitic) magmas by decompression melting of phlogopite+pargasite lherzolite. LITHOS 72, 209–229. https://doi.org/10.1016/j.lithos.2003.09.003

Condamine, P., Médard, E., 2014. Experimental melting of phlogopite-bearing mantle at 1 GPa: Implications for potassic magmatism. Earth and Planetary Science Letters 397, 80–92. https://doi.org/10.1016/j.epsl.2014.04.027

Condamine, P., Médard, E., Devidal, J.-L., 2016. Experimental melting of phlogopite-peridotite in the garnet stability field. Contributions to Mineralogy and Petrology 171, 1–26. https://doi.org/10.1007/s00410-016-1306-0

Dalou, C., Koga, K.T., Le Voyer, M., Shimizu, N., 2014. Contrasting partition behavior of F and Cl during hydrous mantle melting: implications for Cl/F signature in arc magmas. Progress in Earth and Planetary Science 1, 309–17. https://doi.org/10.1186/s40645-014-0026-1

Dalou, C., Koga, K.T., Shimizu, N., Boulon, J., Devidal, J.-L., 2011. Experimental determination of F and Cl partitioning between lherzolite and basaltic melt. Contributions to Mineralogy and Petrology 163, 591–609. https://doi.org/10.1007/s00410-011-0688-2

Dawson J. B. and Smith J. V., 1982. Upper-mantle amphiboles: a review. European Journal of Mineralogy 45, 35–46.

Edgar, A. D., Green, D. H., & Hibberson, W. O., 1976. Experimental Petrology of a Highly Potassic Magma. Journal of Petrology 17(3), 339–356.

Edgar, A. D., Condliffe, E., Barnett, R. L., & Shirran, R. J., 1980. An Experimental Study of an Olivine Ugandite Magma and Mechanisms for the Formation of its K-Enriched Derivatives. Journal of Petrology. 21(3), 475–497.

Edgar, A.D., Lloyd, F.E., Vukadinovic, D., 1994. The role of fluorine in the evolution of ultrapotassic magmas. Mineralogy and Petrology 51, 173–193. https://doi.org/10.1007/bf01159726

Edgar, A.D., Pizzolato, L.A., 1995. An experimental study of partitioning of fluorine between K-richterite, apatite, phlogopite, and melt at 20 kbar. Contributions to Mineralogy and Petrology 121, 247–257. https://doi.org/10.1007/BF02688240

Erlank, A.J., Waters, F.G., Hawkesworth, C., Haggerty, S., Allsopp, H.L., Rickard, R.S., Menzies, M.A., 1987. Evidence for mantle metasomatism in peridotite nodules from the Kimberley pipes, South Africa.

Ernst, W.G., 1978. Petrochemical Study of Lherzolitic Rocks from the Western Alps*. Journal of Petrology 19, 341–392.

Falloon, T.J., Green, D.H., Danyushevsky, L.V., 2007. Crystallization temperatures of tholeiite parental liquids: Implications for the existence of thermally driven mantle plumes, in: Special Paper 430: Plates, Plumes and Planetary Processes. Geological Society of America, pp. 235–260. https://doi.org/10.1130/2007.2430(12)

Fitzpayne, A., Giuliani, A., Maas, R., Hergt, J., Janney, P., Phillips, D., 2019. Progressive metasomatism of the mantle by kimberlite melts: Sr–Nd–Hf–Pb isotope compositions of MARID and PIC minerals. Earth and Planetary Science Letters 509, 15–26.

Fitzpayne, A., Giuliani, A., Phillips, D., Hergt, J., Woodhead, J.D., Farquhar, J., Fiorentini, M.L., Drysdale, R.N., Wu, N., 2018. Kimberlite-related metasomatism recorded in MARID and PIC mantle xenoliths. Mineralogy and Petrology 112, 71–84. https://doi.org/10.1007/s00710-018-0573-z

Flemetakis, S., Berndt, J., Klemme, S., Genske, F., Cadoux, A., Louvel, M., Rohrbach, A., 2020. An Improved Electron Microprobe Method for the Analysis of Halogens in Natural Silicate Glasses. Microsc Microanal 26, 857–866. https://doi.org/10.1017/S1431927620013495

Foley, S.F., 1991. High-pressure stability of the fluor- and hydroxy-endmembers of pargasite and K-richterite. Geochimica et Cosmochimica Acta 55, 2689–2694. https://doi.org/10.1016/0016-7037(91)90386-j

Francis, D.M., 1976. The Origin of Amphibole in Lherzolite Xenoliths from Nunivak Island, Alaska. Journal of Petrology 17, 357–378.

Frezzotti, M.L., Ferrando, S., 2018. The Role of Halogens in the Lithospheric Mantle, in: Harlov, D.E., Aranovich, L. (Eds.), The Role of Halogens in Terrestrial and Extraterrestrial Geochemical Processes: Surface, Crust, and Mantle. Springer International Publishing, Cham, pp. 805–845. https://doi.org/10.1007/978-3-319-61667-4_13

Fumagalli, P., Klemme, S., 2015. 2.02 - Mineralogy of the Earth: Phase Transitions and Mineralogy of the Upper Mantle, in: Schubert, G. (Ed.), Treatise on Geophysics (Second Edition). Elsevier, Oxford, pp. 7–31.

Gazel, E., Plank, T., Forsyth, D.W., Bendersky, C., Lee, C.-T.A., Hauri, E.H., 2012. Lithosphere versus asthenosphere mantle sources at the Big Pine Volcanic Field,

California. Geochemistry, Geophysics, Geosystems 13. https://doi.org/10.1029/2012GC004060

Giuliani, A., Kamenetsky, V.S., Kendrick, M.A., Phillips, D., Goemann, K., 2013. Nickel-rich metasomatism of the lithospheric mantle by pre-kimberlitic alkali-S–Cl-rich C–O–H fluids. Contrib Mineral Petrol 165, 155–171. https://doi.org/10.1007/s00410-012-0801-1

Green, D.H., 1973. Conditions of melting of basanite magma from garnet peridotite. Earth and Planetary Science Letters 17, 456–465. https://doi.org/10.1016/0012-821X(73)90214-8

Green, D.H., Hibberson, W.O., Kovács, I., Rosenthal, A., 2010. Water and its influence on the lithosphere– asthenosphere boundary. Nature Publishing Group 467, 448–451. https://doi.org/10.1038/nature09369

Green, D.H., Hibberson, W.O., Rosenthal, A., Kovács, I., Yaxley, G.M., Falloon, T.J., Brink, F., 2014. Experimental Study of the Influence of Water on Melting and Phase Assemblages in the Upper Mantle. Journal of Petrology 55, 2067–2096. https://doi.org/10.1093/petrology/egu050

Griffin, W.L., Wass, S.Y., HOLLIS, J.D., 1984. Ultramafic Xenoliths from Bullenmerri and Gnotuk Maars, Victoria, Australia: Petrology of a Sub-Continental Crust-Mantle Transition. Journal of Petrology 25, 53–87.

Grützner, T., Klemme, S., Rohrbach, A., Gervasoni, F., Berndt, J., 2018. The effect of fluorine on the stability of wadsleyite: Implications for the nature and depths of the transition zone in the Earth’s mantle. Earth and Planetary Science Letters 482, 236–244. https://doi.org/10.1016/j.epsl.2017.11.011

Grützner, T., Klemme, S., Rohrbach, A., Gervasoni, F., Berndt, J., 2017. The role of F-clinohumite in volatile recycling processes in subduction zones. Geology 45, 443–446. https://doi.org/10.1130/G38788.1

Hanley, J.J., Koga, K.T., 2018. Halogens in Terrestrial and Cosmic Geochemical Systems: Abundances, Geochemical Behaviors, and Analytical Methods, in: Harlov, D.E., Aranovich, L. (Eds.), The Role of Halogens in Terrestrial and Extraterrestrial Geochemical Processes. Springer International Publishing, Cham, pp. 21–121.

Harlov, D.E., Aranovich, L. (Eds.), 2018. The Role of Halogens in Terrestrial and Extraterrestrial Geochemical Processes, Springer Geochemistry. Springer International Publishing, Cham. https://doi.org/10.1007/978-3-319-61667-4

Harlow, G.E., Davies, R., 2004. Status report on stability of K-rich phases at upper-mantle conditions. Presented at the 8th International Kimberlite Conference, pp. 1–5.

Harte, B., 1983. Mantle peridotites and processes—The kimberlite sample. Continental basalts and mantle xenoliths (ed. CJ Hawkesworth & M. Norry) 46–91.

Hauri, E.H., Gaetani, G.A., Green, T.H., 2006. Partitioning of water during melting of the Earth's upper mantle at H2O-undersaturated conditions. Earth and Planetary Science Letters 248, 715–734. https://doi.org/10.1016/j.epsl.2006.06.014

Hirose, K., Kawamoto, T., 1995. Hydrous partial melting of lherzolite at 1 GPa: The effect of H2O on the genesis of basaltic magmas. Earth and Planetary Science Letters 133, 463–473.

Holloway, J.R., Burnham, C.W., 1972. Melting Relations of Basalt with Equilibrium Water Pressure Less Than Total Pressure. Journal of Petrology 13, 1–29. https://doi.org/10.1093/petrology/13.1.1

Ionov, D.A., Hofmann, A.W., 1995. Nb-Ta-rich mantle amphiboles and micas: Implications for subduction-related metasomatic trace element fractionations. Earth and Planetary Science Letters 131, 341–356. https://doi.org/10.1086/669978

Joachim, B., Pawley, A.R., Lyon, I.C., Marquardt, K., Henkel, T., Clay, P.L., Ruzié, L., Burgess, R., Ballentine, C.J., 2015. Experimental partitioning of F and Cl between olivine, orthopyroxene and silicate melt at Earth's mantle conditions. Chemical Geology 416, 65–78. https://doi.org/10.1016/j.chemgeo.2015.08.012

Joachim, B., Stechern, A., Ludwig, T., Konzett, J., Pawley, A.R., Ruzié-Hamilton, L., Clay, P.L., Burgess, R., Ballentine, C.J., 2017. Effect of water on the fluorine and chlorine partitioning behavior between olivine and silicate melt. Contributions to Mineralogy and Petrology 172, 15. https://doi.org/10.1007/s00410-017-1329-1

Kawamoto, T., Hirose, K., 1994. Au-Pd sample containers for melting experiments on iron and water bearing systems. ejm 6, 381–386. https://doi.org/10.1127/ejm/6/3/0381

Kennedy, A.K., Lofgren, G.E., Wasserburg, G.J., 1993. An experimental study of trace element partitioning between olivine, orthopyroxene and melt in chondrules: equilibrium values and kinetic effects. Earth and Planetary Science Letters 115, 177–195.

Kjarsgaard, B.A., Pearson, D.G., Tappe, S., Nowell, G.M., Dowall, D.P., 2009. Geochemistry of hypabyssal kimberlites from Lac de Gras, Canada: Comparisons to a

global database and applications to the parent magma problem. Lithos 112, 236–248. https://doi.org/10.1016/j.lithos.2009.06.001

Klemme, S., O'Neill, H.S.C., 1997. The reaction MgCr2O4 + SiO2 = Cr2O3 + MgSiO3 and the free energy of formation of magnesiochromite (MgCr2O4). Contributions to Mineralogy and Petrology 130, 59–65.

Kushiro, I., Syono, Y., Akimoto, S., 1967. Stability of phlogopite at high pressures and possible presence of phlogopite in the earth's upper mantle. Earth and Planetary Science Letters 3, 197–203.

LaTourrette, T., Hervig, R.L., Holloway, J.R., 1995. Trace element partitioning between amphibole, phlogopite, and basanite melt. Earth and Planetary Science Letters 135, 13–30. https://doi.org/10.1016/0012-821x(95)00146-4

Le Maitre, R.W., Streckeisen, A., Zanettin, B., Le Bas, M.J., Bonin, B., Bateman, P., 2005. Igneous Rocks: A Classification and Glossary of Terms, Recommendations of the International Union of Geological Sciences Subcommission on the Systematics of Igneous Rocks. Cambridge University Press.

Leake, B.E., Woolley, A.R., Arps, C.E.S., Birch, W.D., Gilbert, M.C., Grice, J.D., Hawthorne, F.C., Kato, A., Kisch, H.J., Krivovichev, V.G., Linthout, K., Laird, J., Mandarino, J., Maresch, W.V., Nickel, E.H., Rock, N.M.S., Schumacher, J.C., Smith, D.C., Stephenson, N.C.N., Ungaretti, L., Whittaker, E.J.W., Youzhi, G., 1997. Nomenclature of amphiboles Report of the Subcommittee on Amphiboles of the International Mineralogical Association Commission on New Minerals and Mineral Names. European Journal of Mineralogy 9, 623–651. https://doi.org/10.1127/ejm/9/3/0623

Liu, C.-Z., Wu, F.-Y., Chung, S.-L., Zhao, Z.-D., 2011. Fragments of hot and metasomatized mantle lithosphere in Middle Miocene ultrapotassic lavas, southern Tibet. Geology 39, 923–926.

Locock, A.J., 2014. An Excel spreadsheet to classify chemical analyses of amphiboles following the IMA 2012 recommendations. Computers and Geosciences 62, 1–11. https://doi.org/10.1016/j.cageo.2013.09.011

Lundstrom, C.C., Shaw, H.F., Ryerson, F.J., Williams, Q., Gill, J., 1998. Crystal chemical control of clinopyroxene-melt partitioning in the Di-Ab-An system: implications for elemental fractionations in the depleted mantle. Geochimica et Cosmochimica Acta 62, 2849–2862. https://doi.org/10.1016/S0016-7037(98)00197-5

Medaris, L.G., 1980. Petrogenesis of the Lien peridotite and associated eclogites, Almklovdalen, Western Norway. LITHOS 13, 339–353.

Mengel, K., Green, D., 1989. Stability of Amphibole and Phlogopite in Metasomatised Peridotite under water-saturated and water-undersaturated conditions. Geological Society of Australia 1, 571–581.

Métrich, N., Zanon, V., Créon, L., Hildenbrand, A., Moreira, M., Marques, F.O., 2014. Is the ‘Azores Hotspot’ a Wetspot? Insights from the Geochemistry of Fluid and Melt Inclusions in Olivine of Pico Basalts. Journal of Petrology 55, 377–393. https://doi.org/10.1093/petrology/egt071

Millhollen, G.L., Irving, A.J., Wyllie, P.J., 1974. Melting Interval of Peridotite with 5.7 per Cent Water to 30 Kilobars. The Journal of Geology 82, 575–587.

Mosenfelder, Jed L., Rossman, G.R., 2013. Analysis of hydrogen and fluorine in pyroxenes: I. Orthopyroxene. American Mineralogist 98, 1026–1041. https://doi.org/10.2138/am.2013.4291

Mosenfelder, Jed L, Rossman, G.R., 2013. Analysis of hydrogen and fluorine in pyroxenes: II. Clinopyroxene. American Mineralogist 98, 1042–1054. https://doi.org/10.2138/am.2013.4413

Mysen, B.O., Boettcher, A.L., 1975a. Melting of a Hydrous Mantle: I. Phase Relations of Natural Peridotite at High Pressures and Temperatures with Controlled Activities of Water, Carbon Dioxide, and Hydrogen. Journal of Petrology 16, 520–548. https://doi.org/10.1093/petrology/16.1.520

Mysen, B.O., Boettcher, A.L., 1975b. Melting of a Hydrous Mantle: II. Geochemistry of Crystals and Liquids Formed by Anatexis of Mantle Peridotite at High Pressures and High Temperatures as a Function of Controlled Activities of Water, Hydrogen, and Carbon Dioxide. Journal of Petrology 16, 549–593.

Nickel, K.G., Green, D.H., 1984. The Nature of the Upper-Most Mantle Beneath Victoria, Australia as Deduced from UL Tramafic Xenoliths, in: KORNPROBST, J. (Ed.), Kimberlites. Elsevier, pp. 161–178. https://doi.org/10.1016/B978-0-444-42274-3.50020-2

Niida, K., Green, D.H., 1999. Stability and chemical composition of pargasitic amphibole in MORB pyrolite under upper mantle conditions. Contributions to Mineralogy and Petrology 135, 18–40. https://doi.org/10.1007/s004100050495

Obata, M., Morten, L., 1987. Transformation of Spinel Lherzolite to Garnet Lherzolite in Ultramafic Lenses of the Austridic Crystalline Complex, Northern Italy. Journal of Petrology 28, 599–623.

O'Leary, J.A., Gaetani, G.A., Hauri, E.H., 2010. The effect of tetrahedral Al3+ on the partitioning of water between clinopyroxene and silicate melt. Earth and Planetary Science Letters 297, 111–120. https://doi.org/10.1016/j.epsl.2010.06.011

Piper, D.J.W., Pe-Piper, G., Anastasakis, G., Reith, W., 2019. The volcanic history of Pyrgousa—volcanism before the eruption of the Kos Plateau Tuff. Bull Volcanol 81, 32. https://doi.org/10.1007/s00445-019-1290-0

Portnyagin, M. V., Hoernle, K., Plechov, P., Mironov, N., & Khubunaya, S., 2007. Constraints on mantle melting and composition and nature of slab components in volcanic arcs from volatiles (H2O, S, Cl, F) and trace elements in melt inclusions from the Kamchatka Arc. Earth and Planetary Science Letters 255(1), 53–69.

Putirka, K., Platt, B., 2012. Basin and Range volcanism as a passive response to extensional tectonics. Geosphere 8, 1274–1285.

Putirka, K.D., 2008. Thermometers and Barometers for Volcanic Systems. Reviews in Mineralogy and Geochemistry 69, 61–120. https://doi.org/10.2138/rmg.2008.69.3

Rose-Koga, E.F., Koga, K.T., Moreira, M., Vlastelic, I., Jackson, M.G., Whitehouse, M.J., Shimizu, N., Habib, N., 2017. Geochemical systematics of Pb isotopes, fluorine, and sulfur in melt inclusions from São Miguel, Azores. Chemical Geology 1–46. https://doi.org/10.1016/j.chemgeo.2017.03.024

Rosenthal, A., Hauri, E.H., Hirschmann, M.M., 2015. Experimental determination of C, F, and H partitioning between mantle minerals and carbonated basalt, CO2/Ba and CO2/Nb systematics of partial melting, and the CO2 contents of basaltic source regions. Earth and Planetary Science Letters 412, 77–87. https://doi.org/10.1016/j.epsl.2014.11.044

Saal, A.E., Hauri, E.H., Langmuir, C.H., Perfit, M.R., 2002. Vapour undersaturation in primitive mid-ocean-ridge basalt and the volatile content of Earth's upper mantle. Nature Publishing Group 419, 451–455. https://doi.org/10.1038/nature01073

Salters, V.J.M., Longhi, J., 1999. Trace element partitioning during the initial stages of melting beneath mid-ocean ridges. Earth and Planetary Science Letters 166, 15–30.

Salters, V.J.M., Stracke, A., 2004. Composition of the depleted mantle. Geochemistry, Geophysics, Geosystems 5. https://doi.org/10.1029/2003GC000597

Sato, K., Katsura, T., Ito, E., 1997. Phase relations of natural phlogopite with and without enstatite up to 8 GPa: implication for mantle metasomatism. Earth and Planetary Science Letters 146, 511–526.

Seyler, M., Mattson, P.H., 1989. Petrology and thermal evolution of the Tinaquillo peridotite (Venezuela). Journal of Geophysical Research: Solid Earth 94, 7629–7660. https://doi.org/10.1029/JB094iB06p07629

Shimizu, K., Saal, A.E., Myers, C.E., Nagle, A.N., Hauri, E.H., Forsyth, D.W., Kamenetsky, V.S., Niu, Y., 2016. Two-component mantle melting-mixing model for the generation of mid-ocean ridge basalts: Implications for the volatile content of the Pacific upper mantle. Geochimica et Cosmochimica Acta 176, 44–80. https://doi.org/10.1016/j.gca.2015.10.033

Takahashi, E., 1980. Thermal history of lherzolite xenoliths—I. Petrology of lherzolite xenoliths from the ichinomegata crater, oga peninsula, northeast Japan. Geochimica et Cosmochimica Acta 44, 1643–1658.

Taylor, W.R., 1998. An experimental test of some geothermometer and geobarometer formulations for upper mantle peridotites with application to the thermobarometry of fertile Iherzolite and garnet websterite.

Van den Bleeken, G., Koga, K.T., 2015. Experimentally determined distribution of fluorine and chlorine upon hydrous slab melting, and implications for F–Cl cycling through subduction zones. Geochimica et Cosmochimica Acta 171, 353–373. https://doi.org/10.1016/j.gca.2015.09.030

Varne, R., 1970. Hornblende lherzolite and the upper mantle. Contributions to Mineralogy and Petrology 27, 45–51.

Vigouroux, N., Wallace, P.J., Kent, A.J.R., 2008. Volatiles in High-K Magmas from the Western Trans-Mexican Volcanic Belt: Evidence for Fluid Fluxing and Extreme Enrichment of the Mantle Wedge by Subduction Processes. Journal of Petrology 49, 1589–1618. https://doi.org/10.1093/petrology/egn039

Vukadinovic, D., Edgar, A.D., 1993. Phase relations in the phlogopite-apatite system at 20 kbar; implications for the role of fluorine in mantle melting. Contributions to Mineralogy and Petrology 114, 247–254. https://doi.org/10.1007/bf00307759

Wagner, C., Deloule, E., Mokhtari, A., 1996. Richterite-bearing peridotites and MARID-type inclusions in lavas from North Eastern Morocco: mineralogy and D/H isotopic studies. Contributions to Mineralogy and Petrology 124, 406–421. https://doi.org/10.1007/s004100050200

Wallace, M.E., Green, D.H., 1991. The effect of bulk rock composition on the stability of amphibole in the upper mantle: Implications for solidus positions and mantle metasomatism. Mineralogy and Petrology 44, 1–19. https://doi.org/10.1007/BF01167097

Waters, F.G., 1987. A suggested origin of MARID xenoliths in kimberlites by high pressure crystallization of an ultrapotassic rock such as lamproite. Contributions to Mineralogy and Petrology 95, 523–533. https://doi.org/10.1007/BF00402210

Workman, R.K., Hauri, E.H., Hart, S.R., Wang, J., Blusztajn, J., 2006. Volatile and trace elements in basaltic glasses from Samoa: Implications for water distribution in the mantle. Earth and Planetary Science Letters 241, 932–951. https://doi.org/10.1016/j.epsl.2005.10.028

Wyllie, P.J., Sekine, T., 1982. The formation of mantle phlogopite in subduction zone hybridization. Contributions to Mineralogy and Petrology 79, 375–380. https://doi.org/10.1007/BF01132067

Zhang, C., Koepke, J., Wang, L.-X., Wolff, P.E., Wilke, S., Stechern, A., Almeev, R.R., Holtz, F., 2016. A Practical Method for Accurate Measurement of Trace Level Fluorine in Mg- and Fe-Bearing Minerals and Glasses Using Electron Probe Microanalysis. Geostandards and Geoanalytical Research 40, 351–363. https://doi.org/10.1111/j.1751-908X.2015.00390.x

**"Constraining the presence of amphibole and mica in metasomatized mantle sources th**
Flemetakis S, Klemme S , Stracke A, Genske F, Berndt J, Rohrbach A

Table 1. F, Cl and Br contents of reference glasses and minerals analyzed in the present stu

| Glass/Mineral | Code name | Description | Analytical Method |
|---|---|---|---|
| Glass | VG-2[1] | | EPMA |
| Glass | VG-2[8] | | EPMA |
| Glass | VG-2[11] | | EPMA |
| Glass | VG-2[4] | | SIMS |
| **Glass** | **VG-2[13]** | | **EPMA** |
| Glass | VG-A99[1] | | EPMA |
| Glass | VG-A99[8] | | EPMA |
| Glass | VG-A99[11] | | EPMA |
| Glass | VG-A99[4] | | SIMS |
| Glass | VG-A99[6] | | EPMA |
| **Glass** | **VG-A99[13]** | | **EPMA** |
| Glass | VG-568[7] | | EPMA |
| Glass | VG-568[11] | | EPMA |
| **Glass** | **VG-568[13]** | | **EPMA** |
| Glass | BCR-2G[11] | | EPMA |
| Glass | BCR-2G[5] | | Ion Chrom./ICP-MS |
| **Glass** | **BCR-2G [13]** | | **EPMA** |
| Glass | AC-E[11] | | EPMA |
| Glass | AC-E[5] | | Ion Chrom./ICP-MS |
| Glass | AC-E[10] | | Ion Chrom./TXRF |
| **Glass** | **AC-E[13]** | | **EPMA** |
| Glass | GS-N[11] | | EPMA |
| Glass | GS-N[5] | | Ion Chrom./ICP-MS |
| Glass | GS-N[10] | | Ion Chrom./TXRF |
| **Glass** | **GS-N[13]** | | **EPMA** |
| Glass | DR-N[11] | | EPMA |
| Glass | DR-N[10] | | Ion Chrom./TXRF |
| **Glass** | **DR-N [13]** | | **EPMA** |
| Glass | 47963 [9] | | Noble gases |
| Glass | 47963[2, 3] | | EPMA |
| Glass | 47963 [13] | | **EPMA** |
| **Glass** | **BIR1-G[13]** | | **EPMA** |
| **Glass** | **NIST 610[13]** | | **EPMA** |
| **Glass** | **NIST 612[13]** | | **EPMA** |
| **Glass** | **Astimex-Obsidian[13]** | | **EPMA** |

| | | | |
|---|---|---|---|
| **Glass** | **GSE1-G[13]** | | **EPMA** |
| **Glass** | **BHVO2-G[13]** | | **EPMA** |
| Glass | A500[12] | | SIMS |
| Glass | A500[12] | | LA-ICP-MS |
| **Glass** | **A500[13]** | | **EPMA** |
| Glass | A1000[12] | | SIMS |
| Glass | A1000[12] | | LA-ICP-MS |
| **Glass** | **A1000[13]** | | **EPMA** |
| Glass | RD5000[12] | | SIMS |
| Glass | RD5000[12] | | LA-ICP-MS |
| **Glass** | **RD5000[13]** | | **EPMA** |
| Mineral | USNM 143965 [11] | Hornblende (Kakanui) | EPMA |
| **Mineral** | **USNM 143965 [13]** | **Hornblende (Kakanui)** | **EPMA** |
| Mineral | USNM 111356 [11] | Hornblende (Arenal) | EPMA |
| **Mineral** | **USNM 111356 [13]** | **Hornblende (Arenal)** | **EPMA** |
| **Mineral** | **USNM 1022511 [13]** | **Scapolite** | **EPMA** |
| **Mineral** | **Astimex - Kaersutite [13]** | **Kaersutite** | **EPMA** |
| **Mineral** | **Astimex - Biotite [13]** | **Biotite** | **EPMA** |

Caption:

[1] Thordarson et al., (2016); [2] Kamenetsky et al., (2000); [3] Kamenetskty and Maas (2000); [4] Straub
Witter and Kuehner (2004); [7] Streck and Wacaster (2006); [8] van der Zwan et al., (2012); [9] Kendri
(2016); [12] Cadoux et al., (2017); **[13] Present study**. Errors reported are either 1σ or 2σ depending
Cadoux et al. (2017) are 2σ SE. Minerals errors in our study are 2-S.D. Our results were obtaine

References:


Cadoux, A., Iacono-Marziano, G., Paonita, A., Deloule, E., Aiuppa, A., Eby, G. N., et al. (2017). A
glasses: application to SR-XRF, LA-ICP-MS and SIMS techniques. *Chemical Geology*, 1–44. http:/

Kamenetsky, V. S., & Maas, R. (2002). Mantle-melt Evolution (Dynamic Source) in the Origin of
*Petrology*, *43*(10), 1909–1922.

Kamenetsky, V. S., Everard, J. L., Crawford, A. J., Varne, R., Eggins, S. M., & Lanyon, R. (2000). E
Macquarie Island (SW Pacific). *Journal of Petrology*, *41*(3), 411–430.

Kendrick, M. A., Kamenetsky, V. S., Phillips, D., & Honda, M. (2012). Halogen systematics (Cl, Br
*Acta*, *81*(C), 82–93. http://doi.org/10.1016/j.gca.2011.12.004

Marks, M. A. W., Wenzel, T., Whitehouse, M. J., Loose, M., Zack, T., Barth, M. G., et al. (2012).
*Chemical Geology*, *291*(C), 241–255. http://doi.org/10.1016/j.chemgeo.2011.10.026

Michel, A., & Villemant, B. (2003). Determination of Halogens (F, Cl, Br, I), Sulfur and Water in
163–171. http://doi.org/10.1111/j.1751-908x.2003.tb00643.x

Straub, S. M., & Layne, G. D. (2003). The systematics of chlorine, fluorine, and water in Izu arc
*Cosmochimica Acta*, *67*(21), 4179–4203. http://doi.org/10.1016/S0016-7037(03)00307-7

Streck M. J. and Wacaster S. (2006) Plagioclase and pyroxene hosted melt inclusions in basaltic
*Geothermal Research* **157**, 236–253.

Thordarson T., Self S., Óskarsson N. and Hulsebosch T. (1996) Sulfur, chlorine, and fluorine deg
*Bulletin of Volcanology* **58**, 205–225.

van der Zwan F. M., Fietzke J. and Devey C. W. (2012) Precise measurement of low (<100 ppm)
*Spectrom.* **27**, 1966.

Wang, L.-X., Marks, M. A. W., Keller, J., & Markl, G. (2014). Halogen variations in alkaline rocks
magmatic processes. *Chemical Geology*, *380*, 133–144. http://doi.org/10.1016/j.chemgeo.201

Witter, J. B., & Kuehner, S. M. (2003). A simple empirical method for high-qulaity electron micr
*Mineralogist*, 1–7.

Zhang, C., Koepke, J., Wang, L.-X., Wolff, P. E., Wilke, S., Stechern, A., et al. (2016). A Practical M
Glasses Using Electron Probe Microanalysis. *Geostandards and Geoanalytical Research*, *40*(3),

Zhang, C., Lin, J., Pan, Y., Feng, R., Almeev, R. R., & Holtz, F. (2017). Electron Probe Microanalys
Aluminium, and Comparison with Microbeam Synchrotron X-Ray Fluorescence Spectrometry.

**ırough halogen partitioning experiments"**

ıdy and the literature

| F (ppm) | Error | Cl (ppm) | Error | Br (ppm) | Error |
|---|---|---|---|---|---|
| - | - | 316 | 19 | - | - |
| - | - | 329 | 5 | - | - |
| 301 | 19 | 303 | 20 | - | - |
| 334 | 14 | | | - | - |
| **212** | **86** | **298** | **31** | - | - |
| - | - | 227 | 20 | - | - |
| - | - | 271 | 9 | - | - |
| 874 | 98 | 225 | 14 | - | - |
| 709 | 47 | - | - | - | - |
| 976 | 4 | - | - | - | - |
| **611** | **92** | **213** | **31** | - | - |
| | | 1013 | 53 | - | - |
| 1968 | 56 | 1045 | 35 | - | - |
| **1786** | **92** | **1015** | **39** | - | - |
| 317 | 59 | 99 | 18 | - | - |
| 448 | 3 | 98 | 8 | - | - |
| **167** | **92** | **38** | **27** | - | - |
| 1890 | 64 | 292 | 17 | - | - |
| 1807 | 184 | 162 | 91 | - | - |
| 1962 | 93 | 261 | 22 | - | - |
| **1885** | **93** | **303** | **29** | - | - |
| 920 | 38 | 497 | 20 | - | - |
| 919 | 5 | 349 | 7 | - | - |
| 932 | 31 | 456 | 32 | - | - |
| **966** | **85** | **485** | **31** | - | - |
| 573 | 71 | 521 | 23 | - | - |
| 567 | 97 | 545 | 25 | - | - |
| **585** | **84** | **484** | **32** | - | - |
| - | - | 1356 | - | - | - |
| 780 | - | 1400 | - | - | - |
| **989** | **96** | **1240** | **44** | - | - |
| **0** | **0** | **0** | **0** | - | - |
| **246** | **82** | **377** | **32** | - | - |
| **0** | **0** | **136** | **28** | - | - |
| **1264** | **85** | **3505** | **61** | - | - |

| | | | | | |
|---|---|---|---|---|---|
| **228** | **31** | **1644** | **18** | - | - |
| **305** | **94** | **70** | **28** | - | - |
| - | - | - | - | 381 | 20 |
| - | - | 603 | 7.5 | 423 | 11 |
| - | - | **686** | **37** | **353** | **155** |
| - | - | - | - | 1127 | 48 |
| - | - | - | - | 1102 | 192 |
| - | - | **688** | **38** | **1030** | **163** |
| - | - | - | - | 5638 | 310 |
| - | - | 762.5 | 12.1 | 5355 | 635 |
| - | - | **893** | **40** | **6512** | **204** |
| 1673 | 51 | 237 | 10 | - | - |
| **1697** | **125** | **227** | **40** | - | - |
| 361 | 46 | 208 | 17 | - | - |
| **454** | **79** | **201** | **27** | - | - |
| - | - | **14186** | **300** | - | - |
| **1796** | **89** | **215** | **41** | - | - |
| **2355** | **204** | - | - | - | - |

) and Layne (2003); [5] Michel and Villemant (2003); [6]
ck et al., (2012); [10] Wang et al., (2014); [11] Zhang et al.,
on the study. Errors for the glasses from our study and
d using our calibration lines for F and Br.


new set of standards for in-situ measurement of bromine abundances in natural silicate
//doi.org/10.1016/j.chemgeo.2017.01.012

a Single MORB Suite: a Perspective from Magnesian Glasses of Macquarie Island. *Journal of*

nriched End-member of Primitive MORB Melts: Petrology and Geochemistry of Glasses from

r, I) in Mid-Ocean Ridge Basalts: A Macquarie Island case study. *Geochimica Et Cosmochimica*

The volatile inventory (F, Cl, Br, S, C) of magmatic apatite: An integrated analytical approach.

Seventeen Geological Reference Materials. *Geostandards and Geoanalytical Research*, *27*(2),

front volcanic rocks: Implications for volatile recycling in subduction zones. *Geochimica Et*

: andesites of the current eruption of Arenal volcano, Costa Rica. *Journal of Volcanology and*

;assing and atmospheric loading by the 1783–1784 AD Laki (Skaftár Fires) eruption in Iceland.

) chlorine concentrations in submarine basaltic glass by electron microprobe. *J. Anal. At.*

from the Upper Rhine Graben (SW Germany): Insights into F, Cl and Br behavior during
4.05.003

roprobe analysis of fluorine at trace levels in Fe-bearing minerals and glasses. *American*

Method for Accurate Measurement of Trace Level Fluorine in Mg- and Fe-Bearing Minerals and
351–363. http://doi.org/10.1111/j.1751-908X.2015.00390.x

sis of Bromine in Minerals and Glasses with Correction for Spectral Interference from
*Geostandards and Geoanalytical Research*, *41*(3), 449–457. http://doi.org/10.1111/ggr.12169

Constraining the presence of amphibole and mica in metasomatized mantle sources through halogen partitioning experiments

Flemetakis S, Klemme S , Stracke A, Genske F, Berndt J, Rohrbach A

**Profiles of the experimental runs**

In order to further assess the attainment of equilibrium of our experimental runs we conducted EMPA profile analyses for all phases. These analyses show that amphibole and mica are homogeneous in terms of their chemical composition (Fig. 1 - 6).

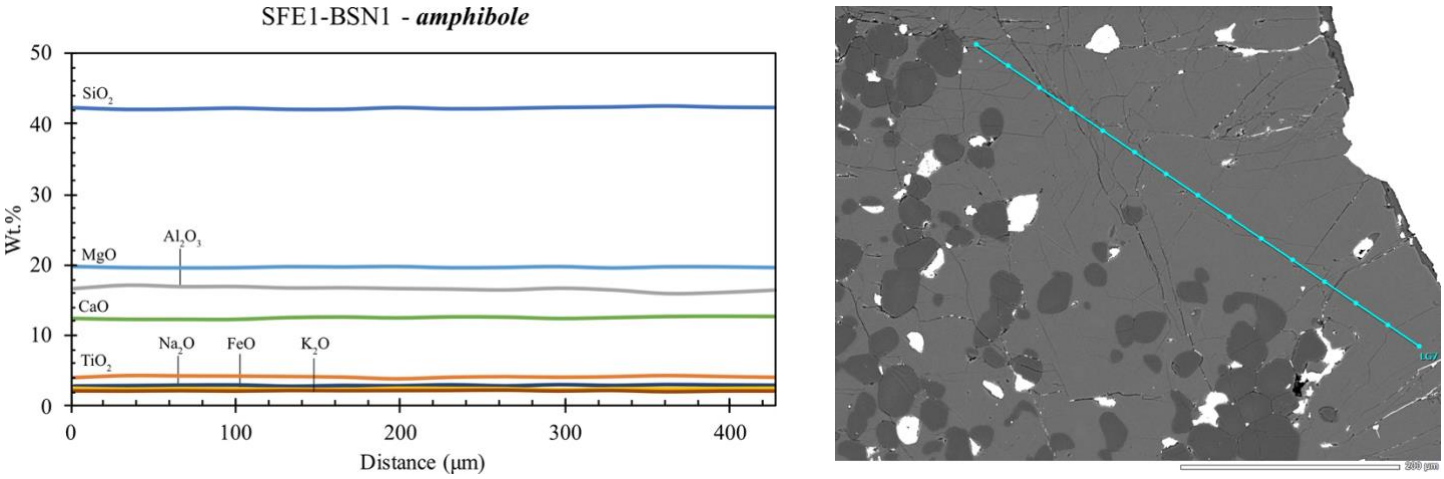


Fig. 1: Profile of amphibole in experiment SFE1-BSN1. Elemental abundances and calculated errors (2-S.D.) can be found in Table 1.

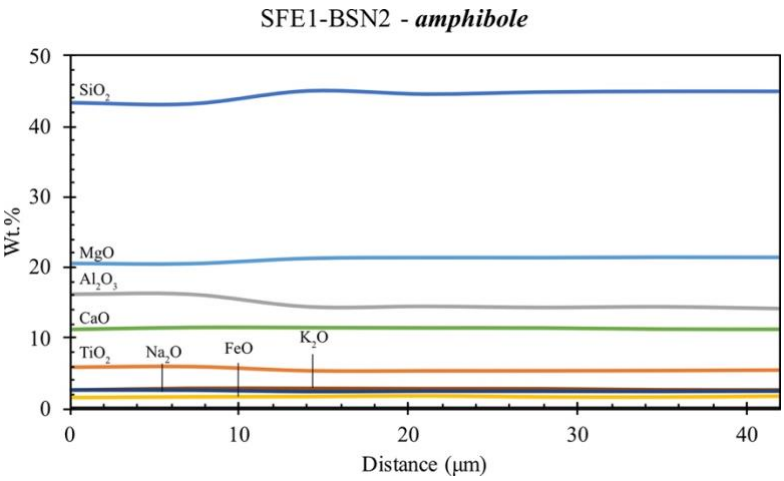


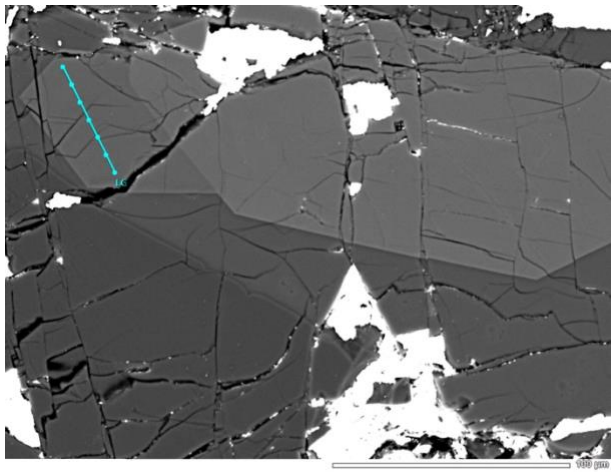

Fig. 2: Profile of amphibole in experiment SFE1-BSN2. Elemental abundances and calculated errors (2-S.D.) can be found in Table 1.

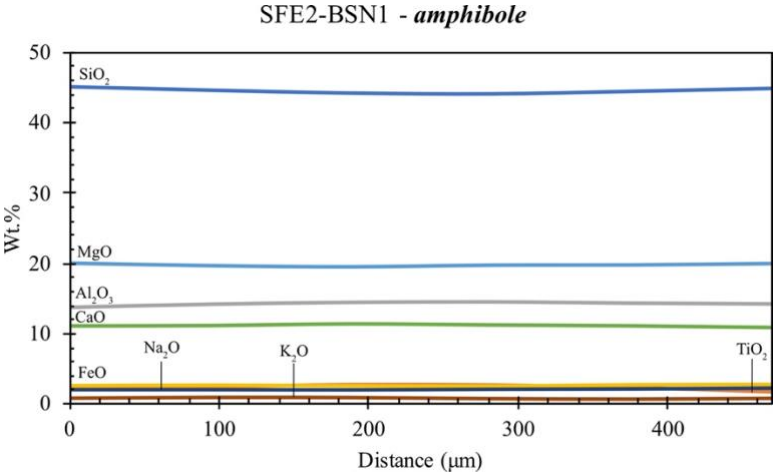


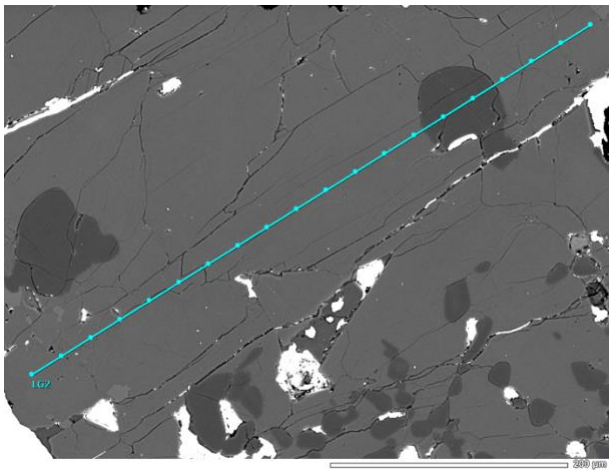

Fig. 3: Profile of amphibole in experiment SFE2-BSN1. Elemental abundances and calculated errors (2-S.D.) can be found in Table 1. The olivine grain analyzed has been excluded from the profile.

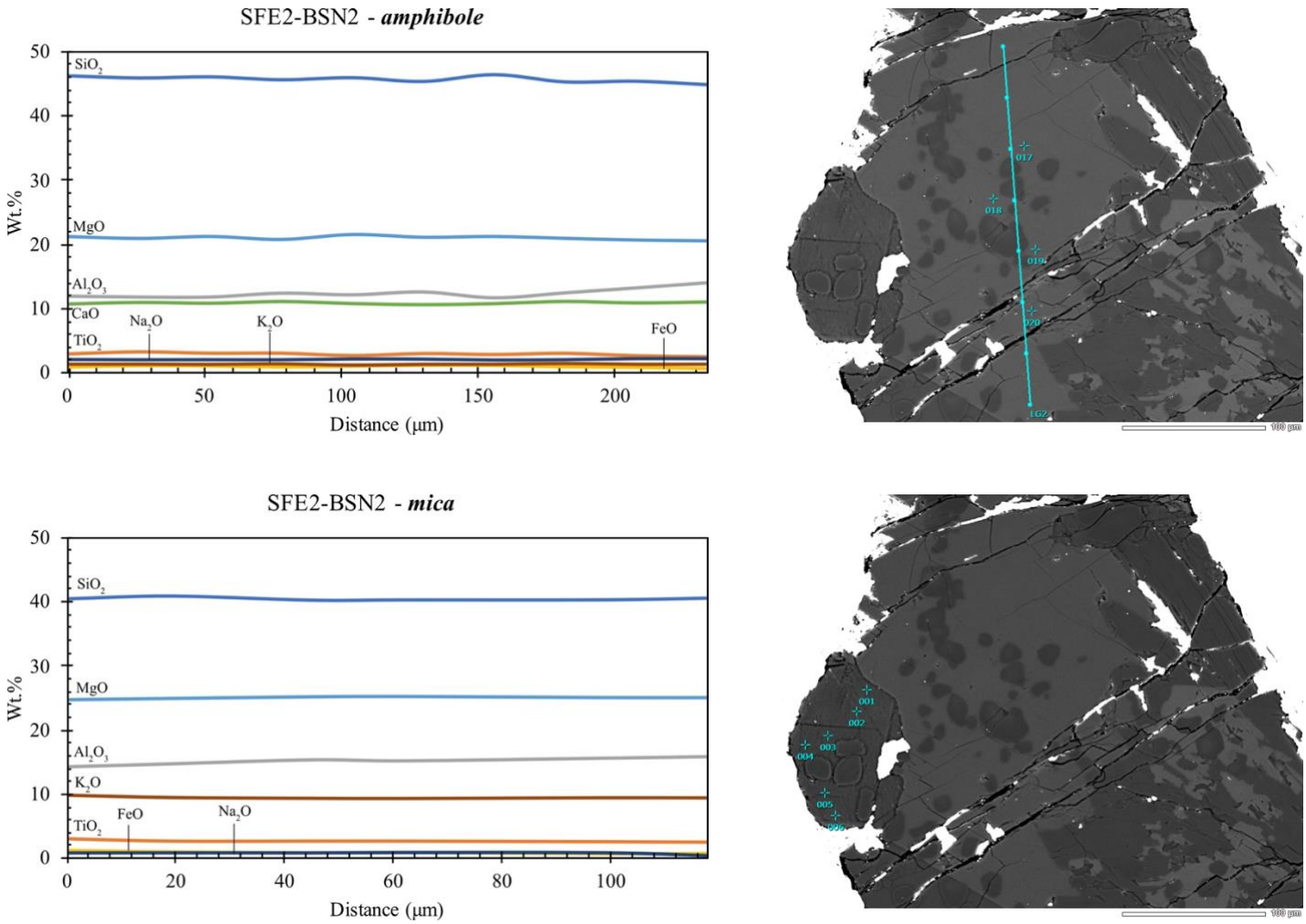


Fig. 4: Upper part, profile of amphibole in experiment SFE2-BSN2. Lower part, profile of mica in experiment SFE2-BSN2. Elemental abundances and calculated errors (2-S.D.), for both phases, can be found in Table 1. The olivine grains analyzed have been excluded from the profile.

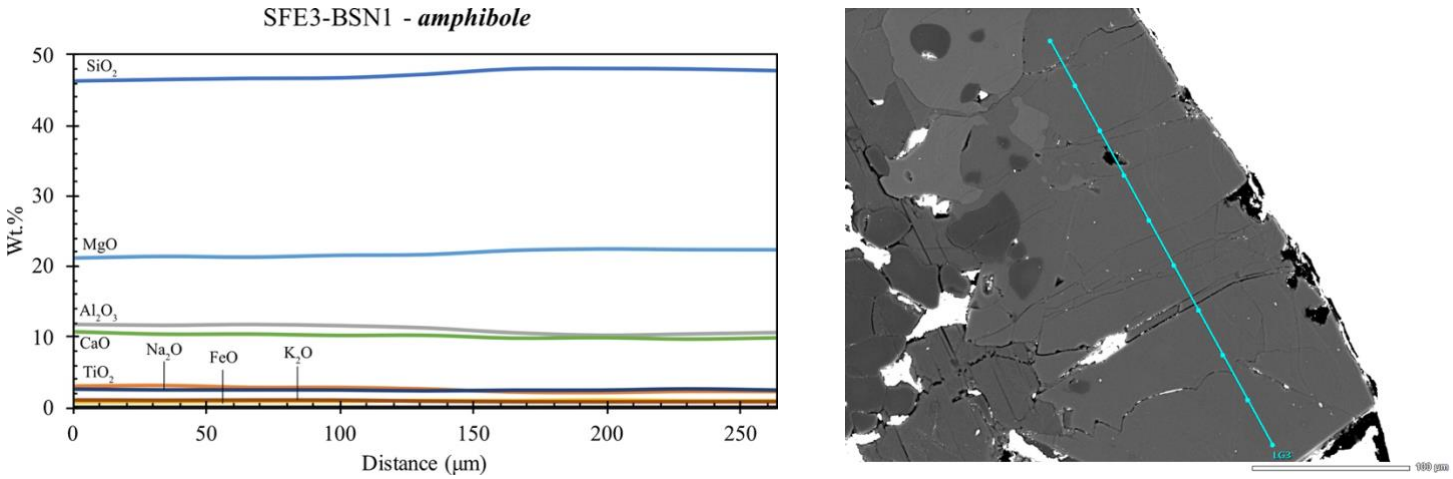


Fig. 5: Upper part, profile of amphibole in experiment SFE3-BSN1. Lower part, profile of mica in experiment SFE3-BSN1. White spots in the BSE image is the Au gold coating of the experiments sample. Elemental abundances and calculated errors (2-S.D.), for both phases, can be found in Table 1.

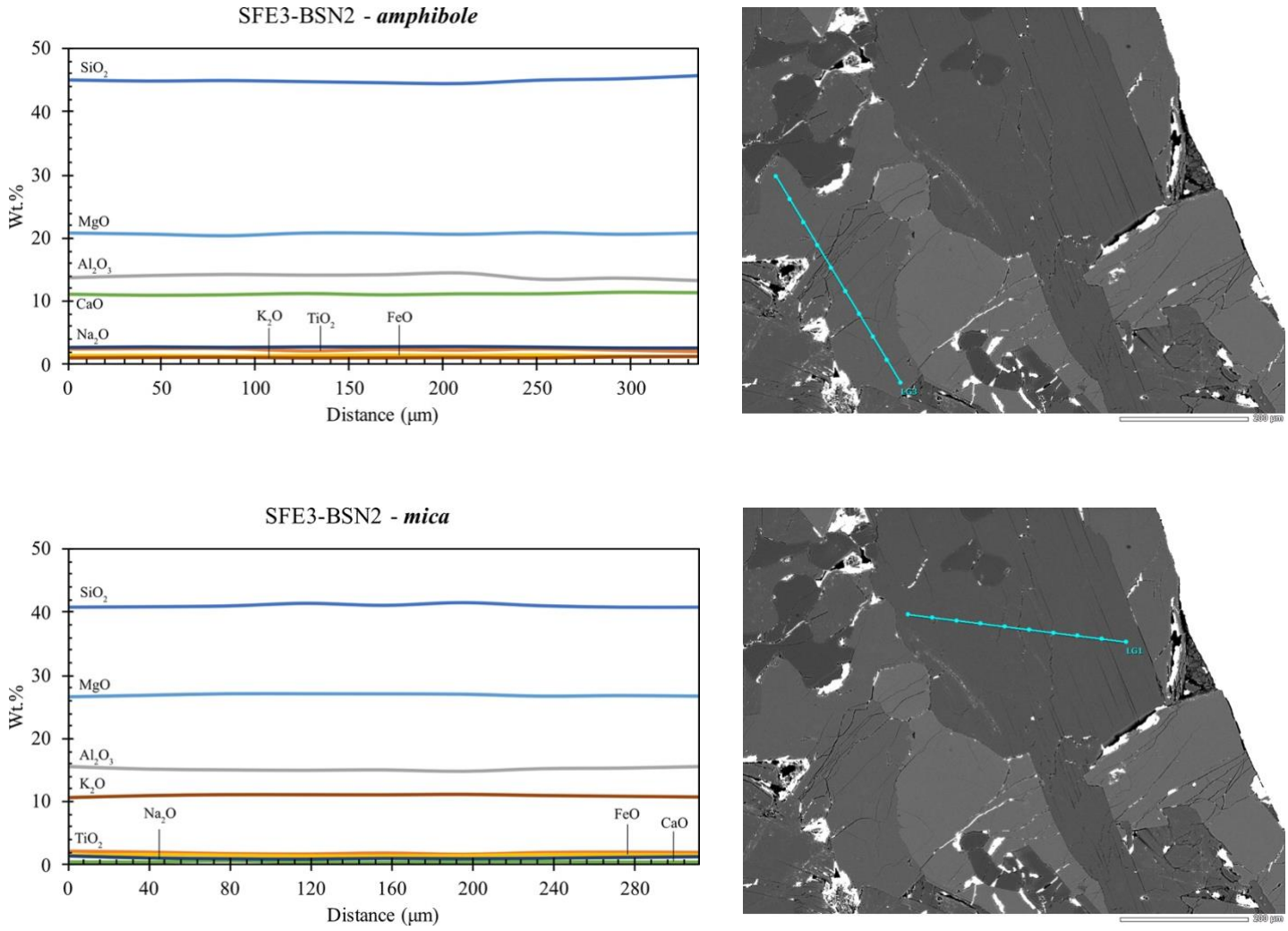


Fig. 6: Upper part, profile of amphibole in experiment SFE3-BSN2. Lower part, profile of mica in experiment SFE3-BSN2. Elemental abundances and calculated errors (2-S.D.), for both phases, can be found in Table 1.

Table 1. Profile-element contents of experimental amphiboles and micas

| Experiment | Mineral | SiO2 | TiO2 | Al2O3 | FeO | MgO | CaO | Na2O | K2O |
|---|---|---|---|---|---|---|---|---|---|
| SFE1-BSN1 | Amph | 42.3(3) | 3.4(2) | 16.1(6) | 1.8(1) | 19.3(2) | 11.9(2) | 2.3(1) | 1.4(2) |
| SFE1-BSN2 | Amph | 44(2) | 4.5(5) | 14(2) | 0.10(1) | 20.4(9) | 10.5(2) | 2.7(2) | 1.4(2) |
| SFE2-BSN1 | Amph | 44.7(7) | 2.3(6) | 14.3(6) | 2.6(2) | 19.8(4) | 11.2(2) | 2.0(1) | 1.00(8) |
| SFE2-BSN2 | Amph | 45.0(8) | 2.9(5) | 12(2) | 1.0(2) | 21.0(6) | 11.0(3) | 2.2(2) | 1.4(2) |
| SFE2-BSN2 | Mica | 40.5(4) | 2.7(5) | 15(1) | 0.9(2) | 25.0(3) | 0.06(6) | 0.8(2) | 9.5(3) |
| SFE3-BSN1 | Amph | 47(2) | 2.7(6) | 11(1) | 1.00(9) | 22(1) | 10.3(7) | 2.7(1) | 0.9(3) |
| SFE3-BSN1 | Mica | 39.9(4) | 3.1(6) | 15.8(7) | 0.5(1) | 25.2(3) | 0.07(7) | 0.5(5) | 11(1) |
| SFE3-BSN2 | Amph | 44.9(8) | 2.4(4) | 14.0(8) | 1.3(2) | 20.6(3) | 11.2(3) | 2.7(2) | 1.0(2) |
| SFE3-BSN2 | Mica | 41.1(5) | 1.3(3) | 14.7(6) | 0.8(1) | 26.7(4) | 0.02(4) | 0.4(2) | 10.5(5) |

Numbers in parentheses represent two standard deviation (2-S.D.) in terms of least units cited

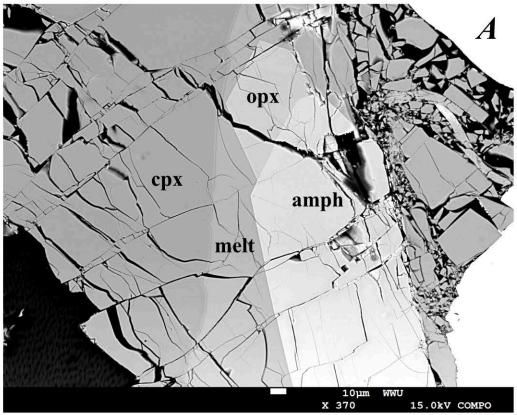
A
opx
cpx
amph
melt
10µm WWU
X 370 15.0kV COMPO

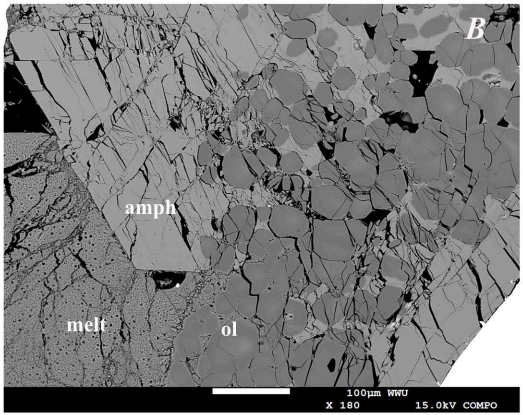
B
amph
melt
ol
100µm WWU
X 180 15.0kV COMPO

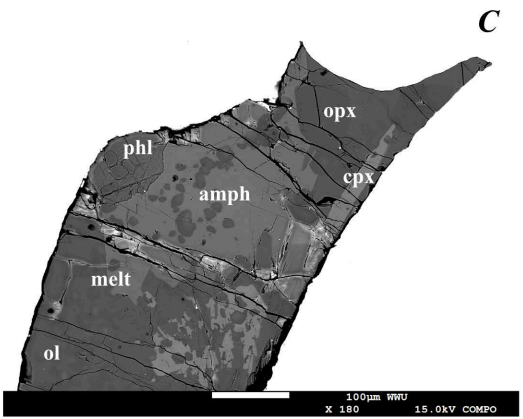
C
opx
phl
cpx
amph
melt
ol
100µm WWU
X 180 15.0kV COMPO

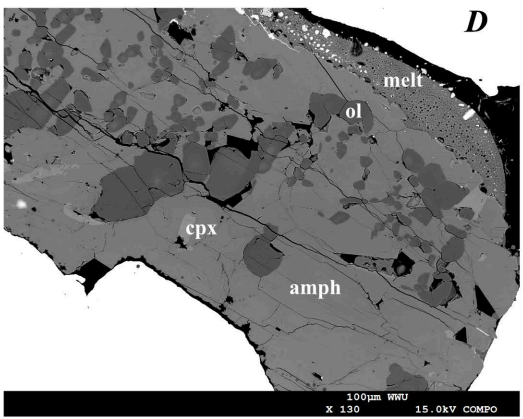
D
melt
ol
cpx
amph
100µm WWU
X 130 15.0kV COMPO

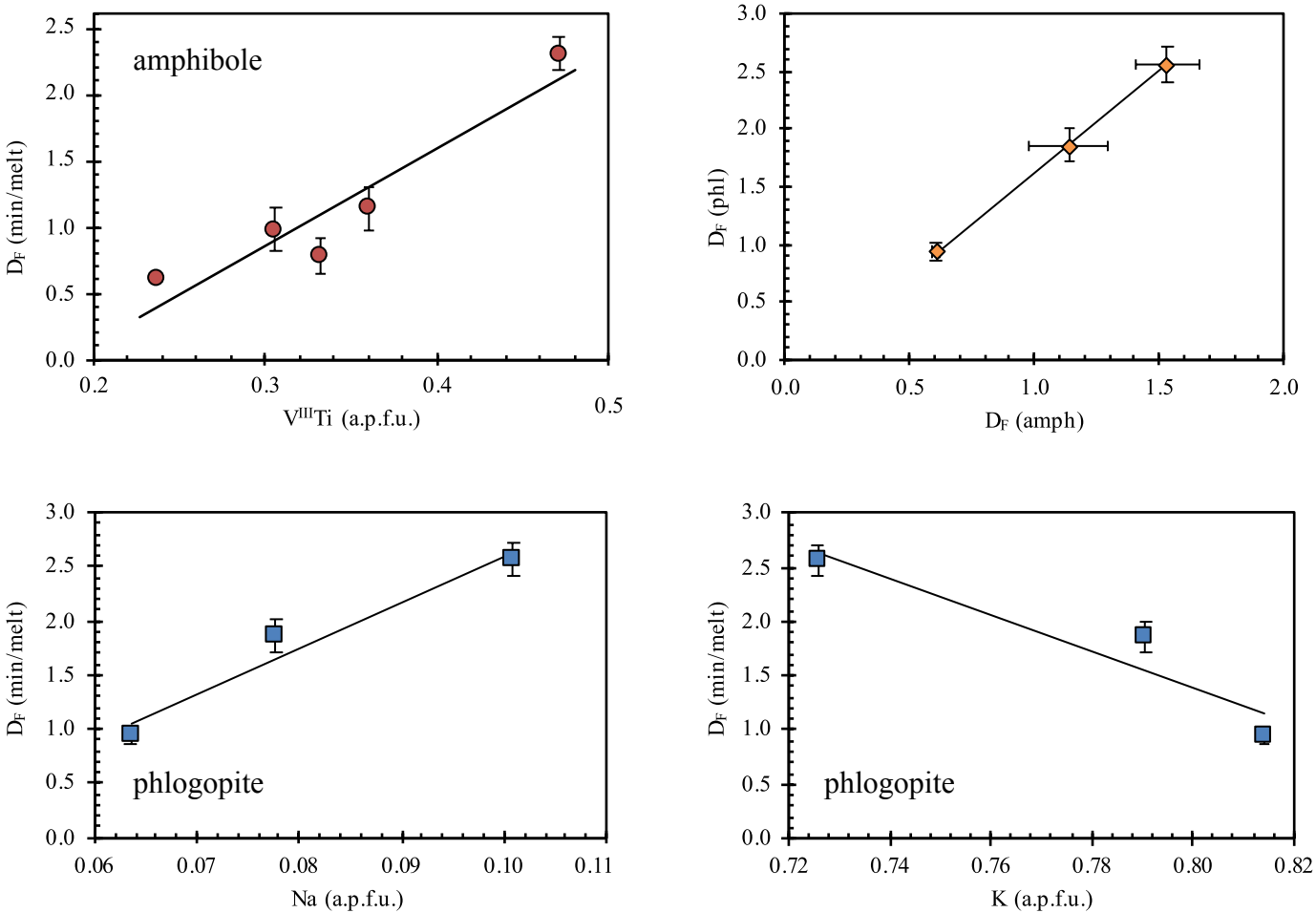
amphibole
$D_F$ (min/melt)
$V^{III}Ti$ (a.p.f.u.)
$D_F$ (phl)
$D_F$ (amph)
phlogopite
$D_F$ (min/melt)
Na (a.p.f.u.)
phlogopite
$D_F$ (min/melt)
K (a.p.f.u.)

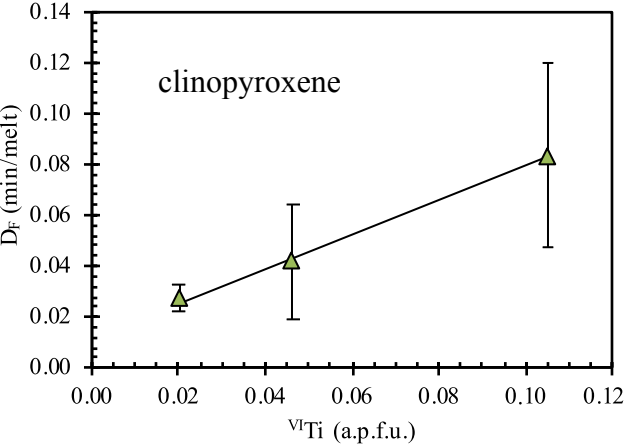
clinopyroxene
$D_F$ (min/melt)
0.00
0.02
0.04
0.06
0.08
0.10
0.12
0.14
0.00
0.02
0.04
0.06
0.08
0.10
0.12
$^{VI}$Ti (a.p.f.u.)

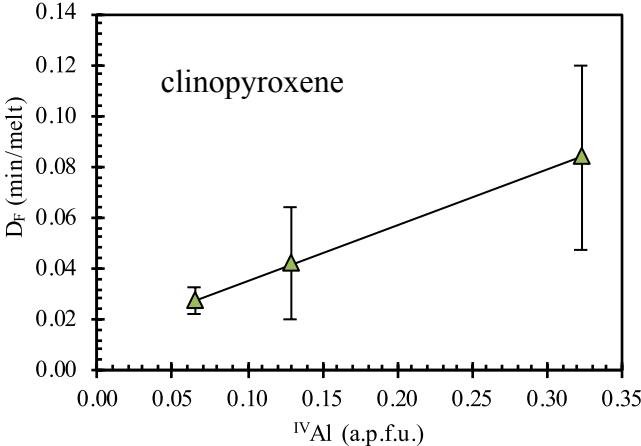
clinopyroxene
$D_F$ (min/melt)
0.00
0.02
0.04
0.06
0.08
0.10
0.12
0.14
0.00
0.05
0.10
0.15
0.20
0.25
0.30
0.35
$^{IV}$Al (a.p.f.u.)

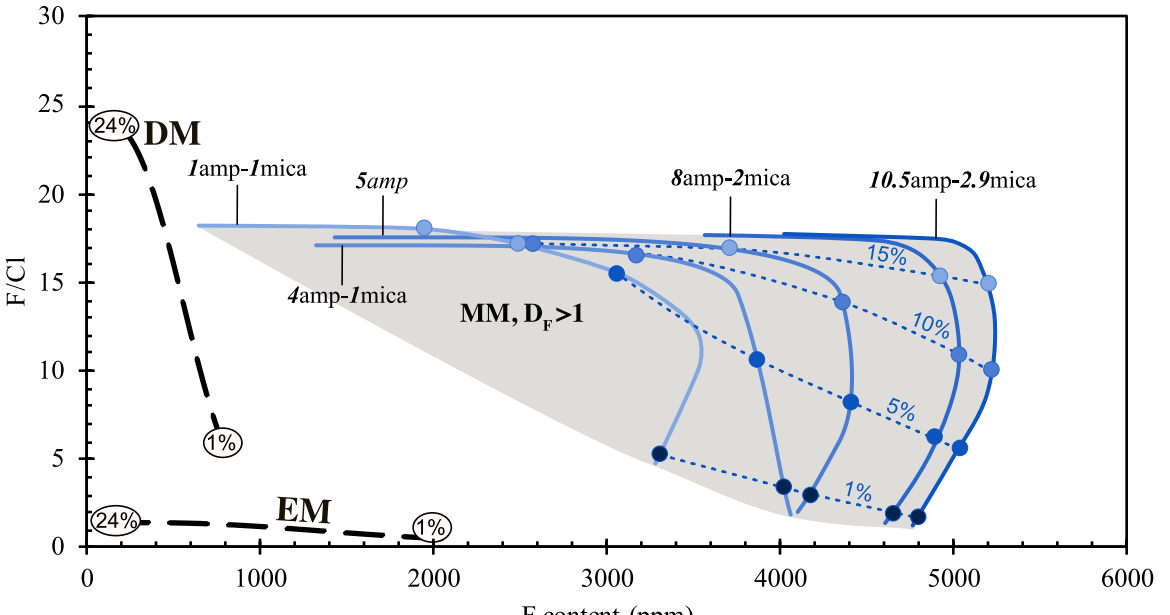
30
25
20
15
10
5
0
F/Cl
0
1000
2000
3000
4000
5000
6000
F content (ppm)
24%
DM
1%
24%
EM
1%
1amp-1mica
5amp
4amp-1mica
8amp-2mica
10.5amp-2.9mica
MM, D_F >1
15%
10%
5%
1%

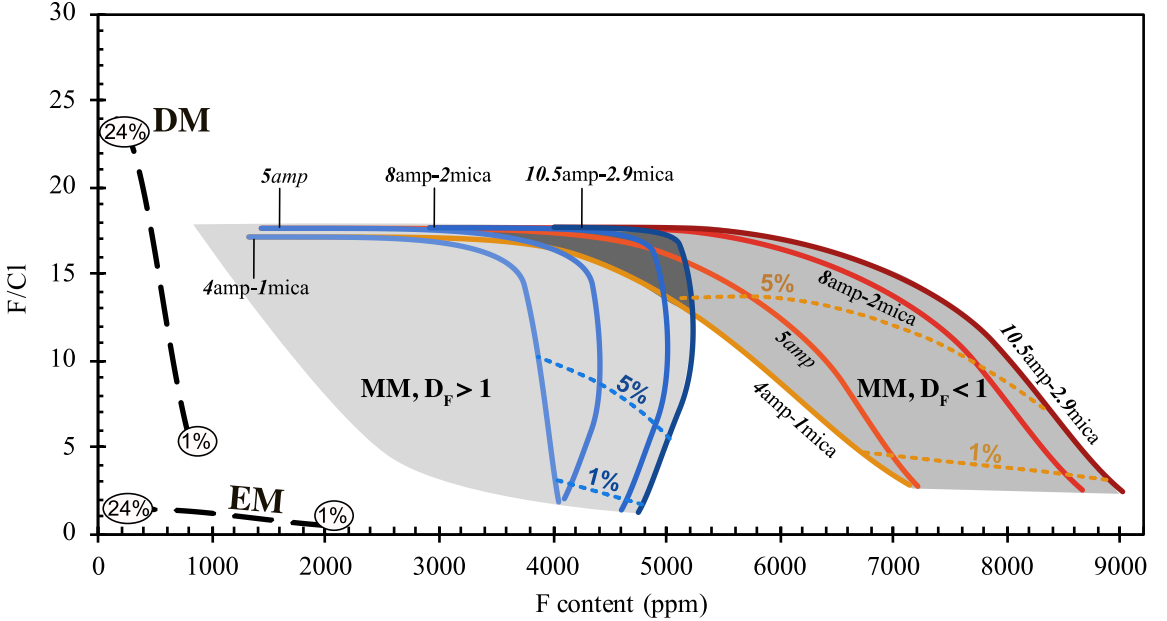
30
25
20
15
10
5
0
F/Cl
0
1000
2000
3000
4000
5000
6000
7000
8000
9000
F content (ppm)
DM
24%
1%
EM
24%
1%
5amp
8amp-2mica
10.5amp-2.9mica
4amp-1mica
MM, D_F > 1
5%
1%
5%
8amp-2mica
5amp
4amp-1mica
MM, D_F < 1
1%
10.5amp-2.9mica

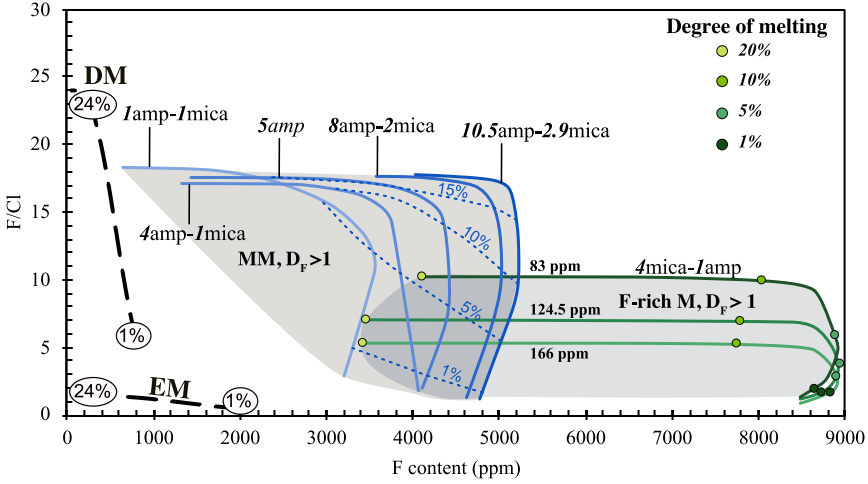
Degree of melting
20%
10%
5%
1%
DM
24%
1%
EM
24%
1%
1amp-1mica
5amp
8amp-2mica
10.5amp-2.9mica
4amp-1mica
MM, D_F>1
15%
10%
5%
1%
83 ppm
124.5 ppm
166 ppm
4mica-1amp
F-rich M, D_F > 1
F/Cl
F content (ppm)
0
5
10
15
20
25
30
0
1000
2000
3000
4000
5000
6000
7000
8000
9000

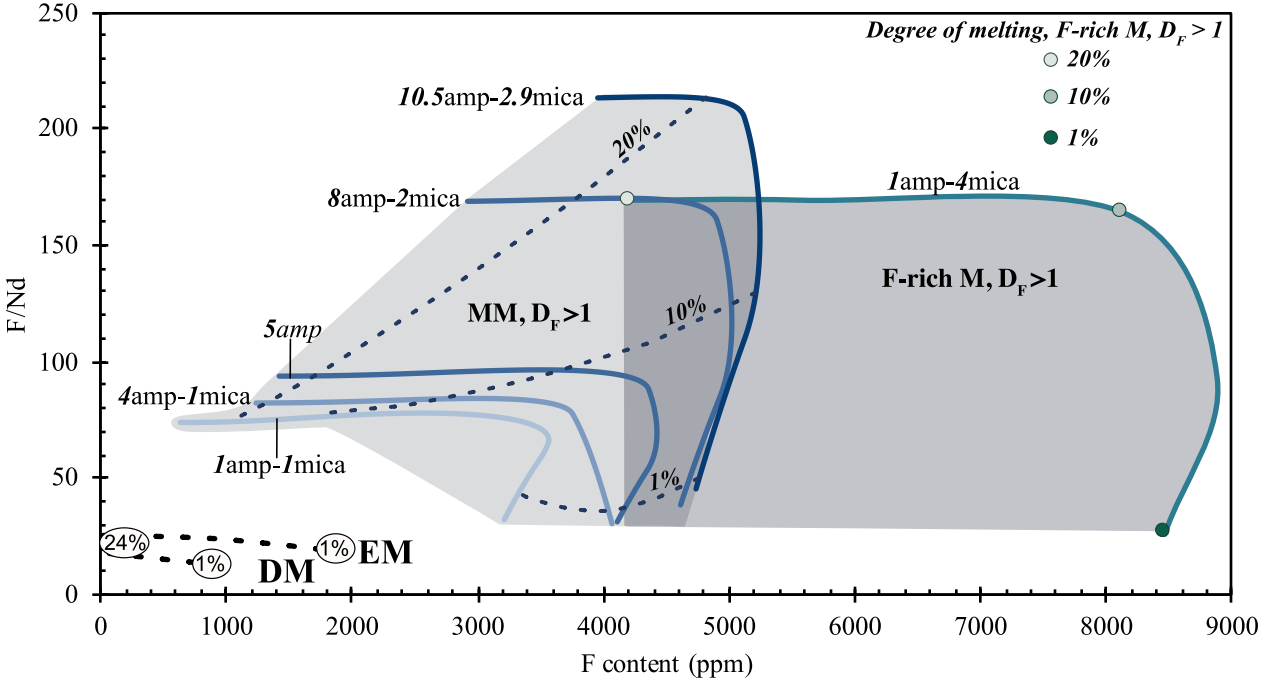
Degree of melting, F-rich M, $D_F > 1$
20%
10%
1%
10.5amp-2.9mica
8amp-2mica
1amp-4mica
5amp
4amp-1mica
1amp-1mica
MM, $D_F$>1
F-rich M, $D_F$>1
20%
10%
1%
24%
1%
1%
DM
EM
F/Nd
F content (ppm)
0
50
100
150
200
250
0
1000
2000
3000
4000
5000
6000
7000
8000
9000

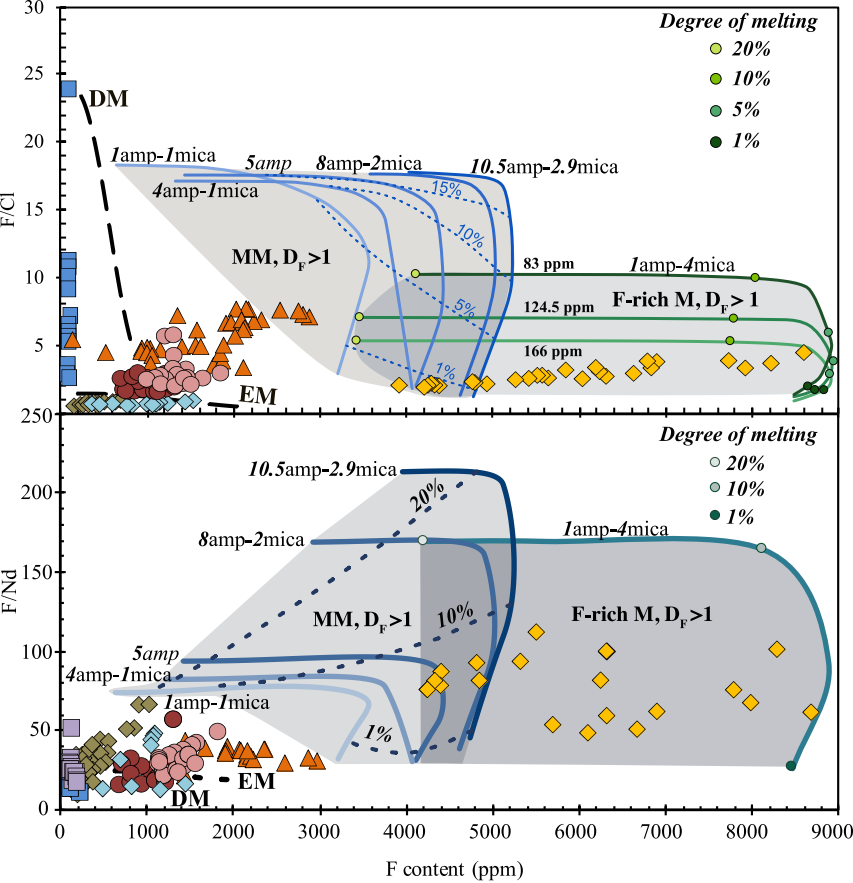
Degree of melting
20%
10%
5%
1%
DM
1amp-1mica
5amp
8amp-2mica
10.5amp-2.9mica
4amp-1mica
15%
10%
5%
1%
MM, D_F>1
83 ppm
1amp-4mica
124.5 ppm
F-rich M, D_F> 1
166 ppm
EM
F/Cl
Degree of melting
20%
10%
1%
10.5amp-2.9mica
20%
8amp-2mica
1amp-4mica
MM, D_F>1
10%
F-rich M, D_F>1
5amp
4amp-1mica
1amp-1mica
1%
EM
DM
F/Nd
F content (ppm)
MORB
Siqueiros Transform Fault 1, 2
Garrett Transform Fault 2
Cont.Intr.
Big Pine Volcanic Field, USA 8
Arc
Aeolian Islands, Italy 5
Kamchatka, Russia 6
W-Transmexican Volc. Belt 7
OIB
Mangaia, Cook Isl. 3
Pico Island, Azores 4